Pergamon

Chaos, Solitons & Fractals Vol. 7, No. 8, pp. 1145–1178, 1996

0960-0779/96 $15.00 + 0.00

0960-0779(95)00114-X

The Pendulum as a Dynamical Billiard

V. V. BELETSKY, G. V. KASATKIN and E. L. STAROSTIN

Keldysh Institute of Applied Mathematics, Russian Academy of Sciences, Miusskaya Sq. 4, Moscow 125047, Russia

(Accepted 17 November 1995)

Abstract—We consider a simple example of a dynamical billiard consisting of a mass point moving in a circle under the influence of a homogeneous gravitational field. The point reflects by the mirror elastic law when it encounters the circular boundary. The problem is integrable between one collision and another, and also when the particle moves on the bounding circle. This makes it possible to build the conditions of existence and stability (in a linear and, at times, in a nonlinear sense, too) of the families of basic periodic trajectories determining the phase space topology for a fixed energy level. The numerical implementation of the Poincaré mapping offers a means of describing the phase pictures with regular and chaotic regions in more detail as well as their evolution as the energy changes. In a weak gravitational field, numerical experiments reveal only periodic trajectories that are symmetric about the vertical diameter of the circle. An analytic proof is given that the imposition of a weak gravitational field causes the disappearance of nonsymmetric two-, three-, four-, and six-link trajectories. The phenomenon arises from the superposition of two factors: the gravitation and the perfect symmetry of the circular billiard. We also consider motion evolution in the special case of the perfectly inelastic reflection law. Copyright © 1996 Elsevier Science Ltd

1. THE SUBJECT OF STUDY AND THE PROBLEM FORMULATION

The problems of present-day mechanics often lead to model tasks on 'dynamical billiards'. They constitute a class of dynamical systems describing motion of a mass point in force fields on an additional condition that there are impact reflections of the mass point from a bounding surface. An orbital probe suspended by the elastic tether or a vehicle jumping on the surface of Phobos (the satellite of Mars) are examples of such dynamical systems. In [1], another billiard in a gravitational field is considered. The uniformly accelerated mass point undergoes elastic collisions with two intersecting planes. This plane model relates to the one-dimensional self-gravitating system which has its origin in astrophysics. It describes stellar motion perpendicular to the galactic plane in very flat galaxies.

It is profitable to use rather simple models for developing an approach to investigation of such systems with collisions.

A simple example of a dynamical billiard is the mass point that moves in a homogeneous gravitational field inside the sphere of a fixed radius which is reflected by the mirror elastic law when it strikes against the surface.

The plane version of this problem is considered in this paper. In standardized variables†, the problem is described as follows:

$$\frac{d^2\mathbf{r}}{dt^2} = -\mathbf{e}, \qquad |\mathbf{r}| \leqslant 1, \qquad \mathbf{v}_+ = \mathbf{v}_- - 2(\mathbf{v}_-\mathbf{n})\mathbf{n}, \tag{1}$$

†The dimensional radius vector $\mathbf{R}$, the velocity $\mathbf{V}$ and time T are related to the dimensionless $\mathbf{r}$, $\mathbf{v}$ and t by the formulas $\mathbf{R} = l\mathbf{r}$, $\mathbf{V} = \sqrt{(lg)}\mathbf{v}$ and $T = \sqrt{(l/g)}t$, where l is the circle radius and g the gravity acceleration.

where $\mathbf{r}$ is the radius vector of the mass point measured from the centre of the circle; $\mathbf{e}$ is the unit vector against the gravity force: $\mathbf{v}_-$ and $\mathbf{v}_+$ are the velocity vectors respectively before and after an elastic collision with the surface; $\mathbf{n}$ is the unit vector, normally and inwardly directed with respect to the surface (in the problem under consideration it is directed to the centre of the circle $\mathbf{n} = -\mathbf{r}/|\mathbf{r}|$).

The energy conservation integral exists:

$$\tfrac{1}{2}v^2 + y = h, \tag{2}$$

where y is the vertical coordinate of the mass point.

The problem given by equation (1) is piecewise integrable (from one collision to another, and also when the mass point moves on the bounding circle $|\mathbf{r}| = 1$). This makes it possible to build the conditions of existence and stability (in a linear and, at times, in a nonlinear sense, too) of the families of basic periodic trajectories determining the phase space topology for a fixed energy level. The numerical implementation of the Poincaré mapping offers a means of describing the phase pictures with regular and chaotic regions in more detail as well as their evolution as the energy level h changes. The computation of the Lyapunov exponents allows conclusions concerning to what extent the trajectories are chaotic. The results of the implementation of this investigation program for the problem (1) are described below.

2. THE BASIC ALGORITHMS OF INVESTIGATION

The phase space of the problem (1) is four-dimensional, but it reduces to three dimensions for a fixed energy level due to the invariant (2). It is convenient to consider a phase trajectory only at the instants when it enters the constraint $|\mathbf{r}| = 1$. Then the phase space degenerates to two-dimensional and the motion can be described by the appropriate Poincaré mapping.

Let the centre of the circle $|\mathbf{r}| = 1$ be the origin of the Cartesian coordinate system (x, y), the x- and y-axes being directed horizontally and upright, respectively. Denote the phase coordinates at the beginning of the n-th segment of the trajectory by $\{x_n, y_n, \dot{x}_n, \dot{y}_n\}$. Starting values of the coordinates are supposed to lie on the circle $|\mathbf{r}| = 1$ and starting values of the velocities are calculated by using the perfectly elastic collision law.

A consecutive algorithm of determination of the starting data for the $(n+1)$-th segment from the starting data for the n-th segment begins with the computation of a time interval τ of the flight duration for the n-th segment as the minimal root of the cubic equation

$$\tau^3 - 4\dot{y}_n\tau^2 + 4(\dot{x}_n^2 + \dot{y}_n^2 - y_n)\tau + 8(x_n\dot{x}_n + y_n\dot{y}_n) = 0. \tag{3}$$

Then the coordinates and velocities are evaluated sequentially by the following formulas:

$$x_{n+1} = \dot{x}_n\tau + x_n, \qquad y_{n+1} = -\tfrac{1}{2}\tau^2 + \dot{y}_n\tau + y_n, \tag{4}$$

$$\begin{aligned} \dot{x}_{n+1} &= \dot{x}_n(y_{n+1}^2 - x_{n+1}^2) - (\dot{y}_n - \tau)2x_{n+1}y_{n+1}, \\ \dot{y}_{n+1} &= -2x_{n+1}y_{n+1}\dot{x}_n - (\dot{y}_n - \tau)(y_{n+1}^2 - x_{n+1}^2). \end{aligned} \tag{5}$$

Equations (4) and (5) are obtained by the integration of equation (1) with the formula for the change of the velocity at the moment of a collision. Equation (3) is derived from the condition $x_{n+1}^2 + y_{n+1}^2 = 1$ by substitution of the right-hand sides of (4) with regard to $x_n^2 + y_n^2 = 1$.

The trajectories (4) and (5) have only a discrete set of points on the circle $|\mathbf{r}| = 1$. The trajectories that contain segments of continuous pendulum-like motion along the circle are not formally considered. By numerical solution of the problem (3), (4) and (5), the

segments of motion along the circle coming off inwards from it are approximated by motion along a chain of an arbitrarily large number of arbitrarily small parabolic arcs.

To study the existence and stability of periodic solutions it is useful to eliminate time τ from equations (4) and (5) and to introduce the polar coordinates: $x = r\sin\alpha$, $y = -r\cos\alpha$. The polar angle α is measured counter-clockwise from the gravity force direction; $-\pi \leqslant \alpha \leqslant +\pi$.

Introducing the designations $a = \dot{\alpha}$, $b = -\dot{r}$, we obtain, instead of (4) and (5), the following equations:

$$a_{n+1}\cos\alpha_{n+1} + b_{n+1}\sin\alpha_{n+1} = a_n\cos\alpha_n - b_n\sin\alpha_n, \tag{6}$$

$$\tfrac{1}{2}(b_{n+1}^2 - a_{n+1}^2)\sin 2\alpha_{n+1} + a_{n+1}b_{n+1}\cos 2\alpha_{n+1} - \sin\alpha_{n+1} = \tfrac{1}{2}(b_n^2 - a_n^2)\sin 2\alpha_n - a_n b_n\cos 2\alpha_n - \sin\alpha_n, \tag{7}$$

$$\tfrac{1}{2}(a_{n+1}^2 + b_{n+1}^2) - \cos\alpha_{n+1} = \tfrac{1}{2}(a_n^2 + b_n^2) - \cos\alpha_n. \tag{8}$$

Equations (6) to (8) link implicitly the coordinate angle α and the velocities a and b at the n-th and $(n+1)$-th points on the circle $r = 1$. Then (8) represents a discrete form of the energy conservation invariant (2).

Along with equations (6) to (8), we consider their linearized form. We introduce the following abbreviations for variations of the angle and the velocities:

$$\delta_n = \delta\alpha_n, \qquad p_n = \delta a_n, \qquad q_n = \delta b_n.$$

Variation of equations (6) to (8) yields

$$P_{n+1}(\alpha_{n+1}, a_{n+1}, b_{n+1})\begin{pmatrix}\delta_{n+1}\\ p_{n+1}\\ q_{n+1}\end{pmatrix} = Q_n(\alpha_n, a_n, b_n)\begin{pmatrix}\delta_n\\ p_n\\ q_n\end{pmatrix}.$$

Here, the matrices P and Q are given by

$$\begin{pmatrix} -a\sin\alpha \pm b\cos\alpha & \cos\alpha & \pm\sin\alpha \\ (b^2 - a^2)\cos 2\alpha \mp 2ab\sin 2\alpha - \cos\alpha & -a\sin 2\alpha \pm b\cos 2\alpha & \pm a\cos 2\alpha + b\sin 2\alpha \\ \sin\alpha & a & b \end{pmatrix},$$

the upper signs corresponding to the matrix P and the lower ones corresponding to the matrix Q.

Definition. A periodic solution is called a k-link if it is described by k points of the Poincaré map of the plane $(\alpha, \dot{\alpha})$ (h fixed).

Stability or instability of a k-link periodic motion is determined by the eigenvalues λ of a matrix Ω, which are the roots of the characteristic equation

$$\det||\Omega - \lambda E|| = 0, \tag{9}$$

where the matrix Ω is given by

$$\Omega = P_0^{-1}Q_{k-1}P_{k-1}^{-1}Q_{k-2}\cdots P_1^{-1}Q_0.$$

Note that

$$\det||P|| = \det||Q|| = b, \qquad \det||\Omega|| = b_0^{-1}b_{k-1}b_{k-1}^{-1}\cdots b_0 = 1.$$

The characteristic equation (9) can be brought into the form

$$(1 - \lambda)(\lambda^2 + 2s\lambda + 1) = 0. \tag{10}$$

The roots of equation (10) satisfy $|\lambda| = 1$ if $|s| \leq 1$. The periodic solution under consideration is then stable in the linear sense [2]. There is an instability for $|s| > 1$. Thus, we need to evaluate s. Sometimes this can be done analytically and sometimes numerically. The presence of the root $\lambda = 1$ in equation (10) is associated with the existence of the energy conservation invariant. By virtue of its existence the periodic trajectories described below are not isolated but they form groups of one-parameter families.

In order to investigate the existence, stability and other properties of periodic trajectories, it is sometimes useful to introduce auxiliary billiards (the vertical semi-circle with the vertical diameter as a wall etc.). Some results below were obtained by using such approaches.

3. PERIODIC SOLUTIONS, THEIR PROPERTIES AND STABILITY

In what follows some one-parameter families of periodic motions and their properties are presented. The initial value of the angle $\alpha = \alpha_0$ on the circle $r = 1$ for a periodic solution may be taken as a parameter. Then the starting components of the velocity will be functions of the angle α_0 and, hence, the energy $h = h(\alpha_0)$. Another type of family has a fixed initial value $\alpha_0 = \alpha_*$, the parameter being one of the components of the initial velocity and consequently the energy level h itself. In either case, it is convenient to consider curves $h(\alpha_0)$ on the plane (α_0, h), $0 \leq \alpha_0 \leq \pi$, $-1 \leq h < \infty$, that correspond to periodic solutions and to mark intervals of stability and instability on these curves (Fig. 1, the stability intervals are drawn bold). Note that, due to the symmetry properties of the homogeneous gravity field, any periodic trajectory with α_0 is accompanied by a trajectory from the same family with $-\alpha_0$.

The energy conservation (2) implies the region of possible motion on plane $(\alpha, \dot{\alpha})$

$$\tfrac{1}{2}\dot{\alpha}^2 - \cos\alpha \leq h, \qquad h = \tfrac{1}{2}(a_0^2 + b_0^2) - \cos\alpha_0, \qquad a_0 = \dot{\alpha}_0, \qquad b_0 = -\dot{r}_0. \tag{11}$$

The sign of equality in (11) corresponds to the pure pendulum-like motion $\dot{r} \equiv 0$ along the circle $r = 1$ with given h. Such motions are not considered (unless otherwise explicitly stated). Inequality (11) implies that the region corresponding to real motions is $h \geq -\cos\alpha_0$ in the plane (α_0, h) (Fig. 1).

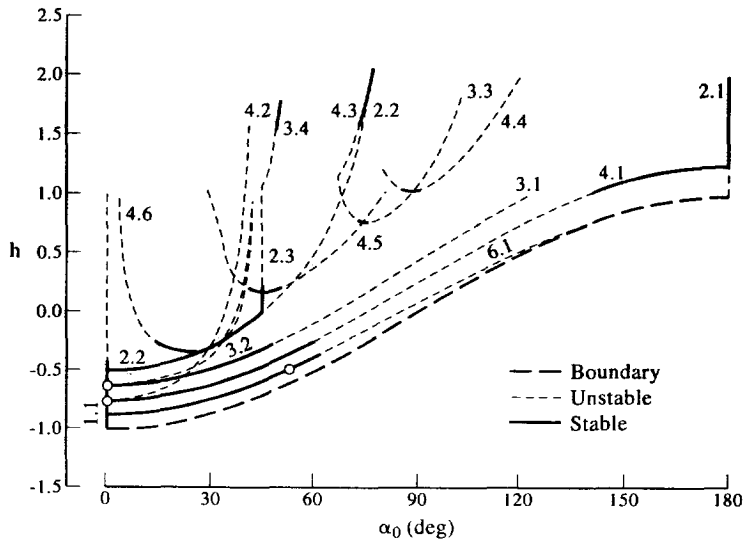

Fig. 1. The diagram of periodic solutions and their stability.

We will describe the families of periodic trajectories in order of increasing number of their links.

Definition. The phase coordinates of the trajectory on the circle $r = 1$ at the beginning of the i-th segment are called the i-th node $u_i = (\alpha_i, a_i, b_i)$.

Each family is indexed $k.m$, where k is the number of links, m the serial number among the set of families with k links. The corresponding curve on the plane (α_0, h) (Fig. 1) as well as images of trajectories (Fig. 2) are labelled with the same index. The description of each family will be presented according to the following plan: the nodes (the symbol **U:**), the existence conditions (the symbol ∃**:**), the stability conditions (the symbol **St:**), the characteristic properties of the trajectories of the family (the symbol **Δ:**), the graph of the trajectory and the sketch of the Poincaré map on the plane $(\alpha, \dot{\alpha})$ for this trajectory.

Recall that the Poincaré map gives the phase variables α, $\dot{\alpha}$ at the moments of successive bounces from the circle $r = 1$, an energy level h being fixed.

The linear theory of stability does not answer the question about the size of 'stability islands', the centres of which are the phase plane points that represent a stable periodic solution. Therefore, the stability islands (the islands of regular motions in the chaotic sea) are drawn in the schematic pictures only symbolically—by small vicinities of periodic points. A more precise picture may be obtained by detailed numerical computation of the Poincaré sections (see Section 5).

1. *One-link trajectories*

1.1. Vertical bounces at the lowest point of the circle without reaching the upper part of the bounding circle (1.1 in Fig. 2).

U: $u_0 = (\alpha_0 = 0,\ a_0 = 0,\ b_0 \neq 0$—the parameter).

∃**:** $\alpha \equiv 0,\ -1 < h < 1$.

St: The parameter of the characteristic equation (10) $s = 2b_0^2 - 1$. This implies that, for $-1 < h < -0.5$, the bounce is stable to a first approximation and unstable for $-0.5 < h < 1$ [3, 4] (Fig. 1).

Δ: (a) This is the only family of one-link trajectories.

(b) The bounce with $h = -0.625$, stable to a first approximation, is resonant in the sense that the roots of the characteristic equation (10) $\lambda_{1,2} = \cos\frac{2}{3}\pi \pm i\sin\frac{2}{3}\pi$ correspond to the rotation of the phase space of the variables δ, p, q through $2\pi/3$ about the eigenvector $\mathbf{e}_q = (0, 0, 1)$ which associates with the third root $\lambda_3 = 1$. Three such rotations result in an identity transformation of the phase space $(\lambda_1^3 = \lambda_3 = 1)$. This singular case corresponds to a bifurcation (Fig. 1) with a birth of two subfamilies of stable three-links *3.1* and two subfamilies of unstable three-links *3.2* (see below).

(c) The bounce with $h = -0.75$, stable to a first approximation, is resonant in the sense that the roots of the characteristic equation (10) $\lambda_{1,2} = \cos(\pi/2) \pm i\sin(\pi/2)$, $\lambda_3 = 1$ fit the resonant relationship $\lambda_1^4 = \lambda_3$. The phase space of the variables δ, p, q transforms identically into itself by the four rotations through the angle $\pi/2$ about the axis q. This singular case corresponds to a bifurcation (Fig. 1) with a birth of a subfamily of stable four-links *4.1* and a subfamily of unstable four-links *4.2* (see below).

2. *Two-link trajectories*

All two-link periodic trajectories are reduced to three families *2.1*, *2.2*, *2.3* listed below.

(a)

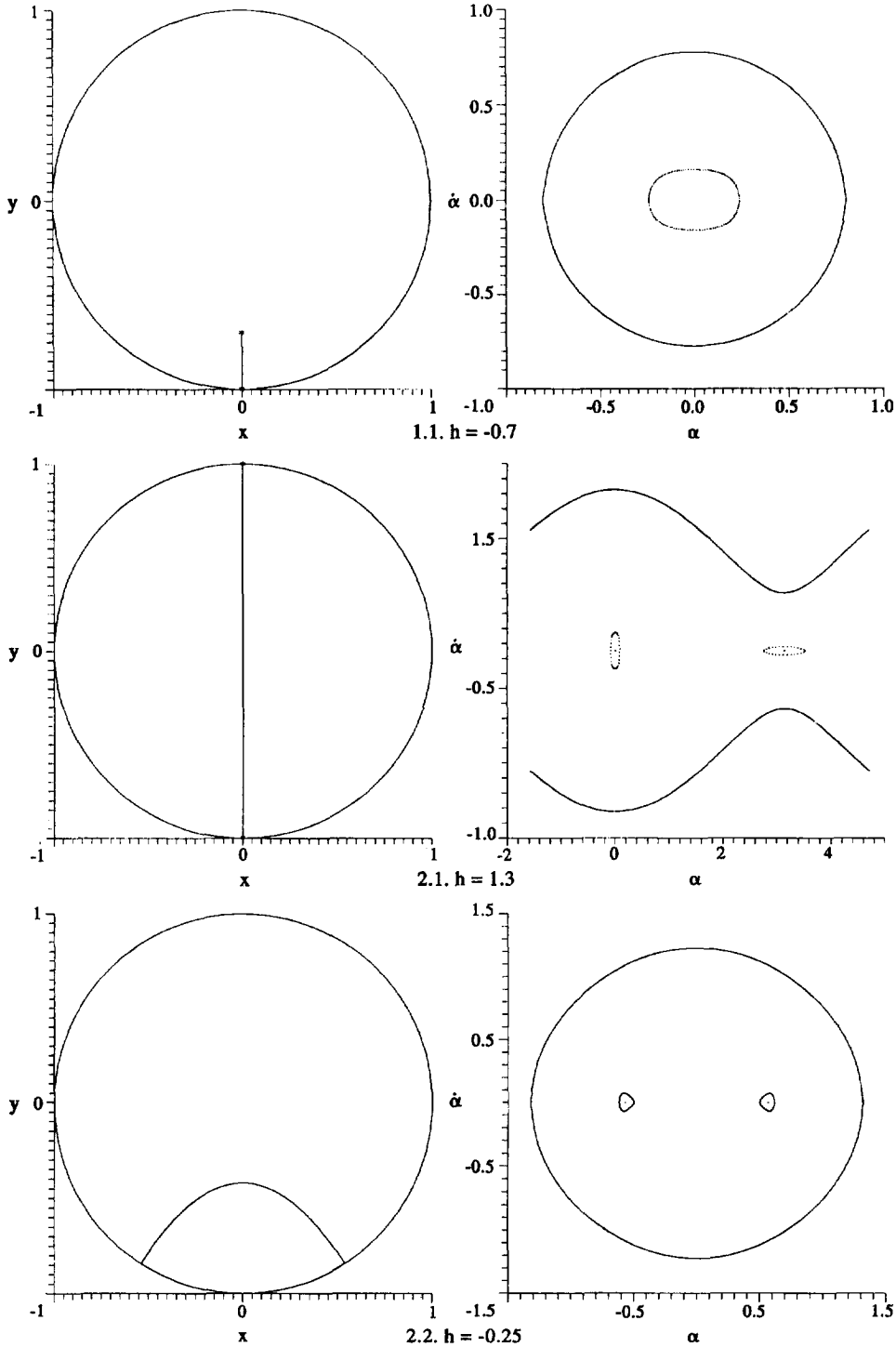

Fig. 2(a). *Caption on p. 1156.*

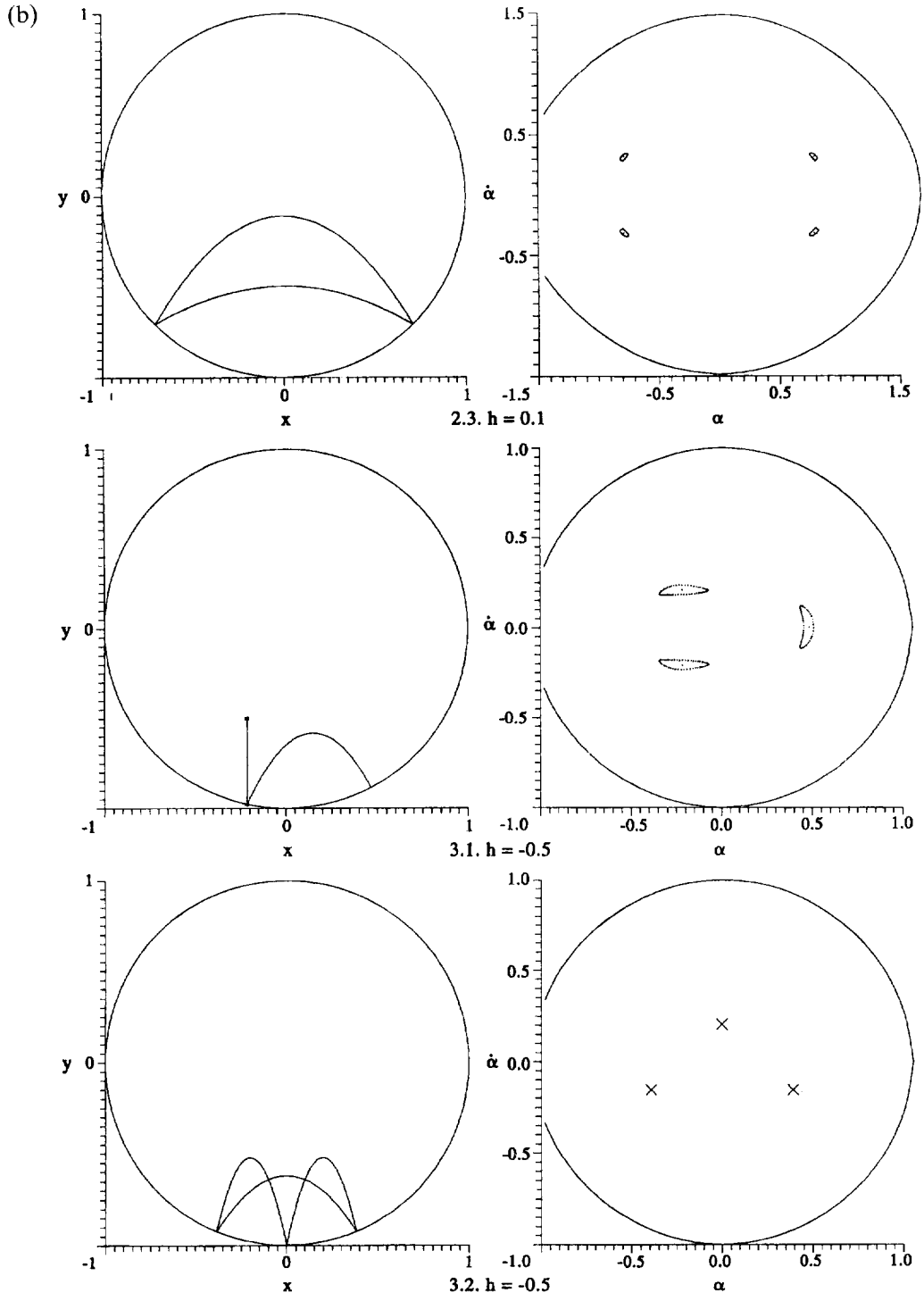

Fig. 2(b). *Caption on p. 1156.*

(c)

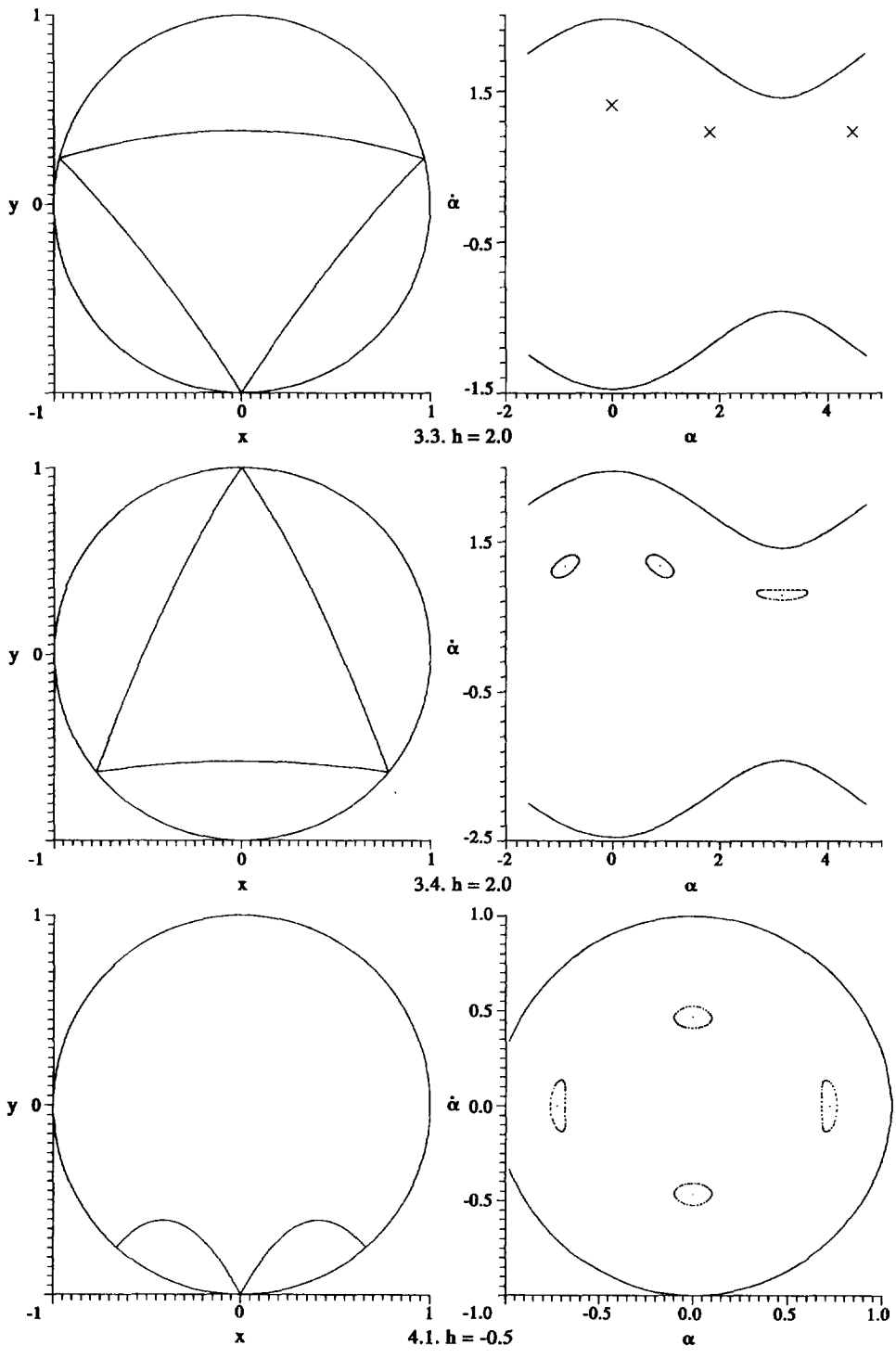

Fig. 2(c). *Caption on p. 1156.*

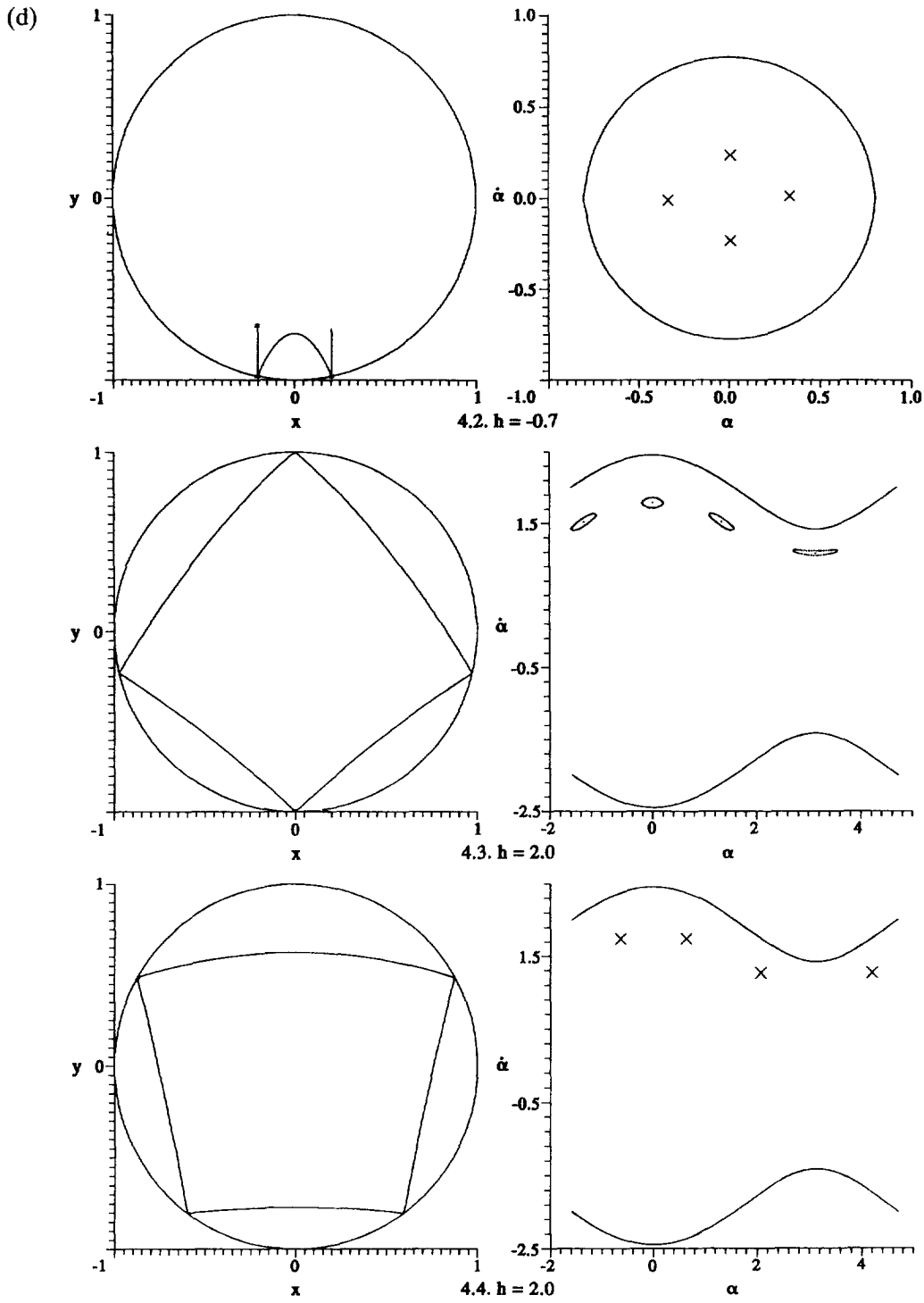

Fig. 2(d). *Caption on p. 1156.*

(e)

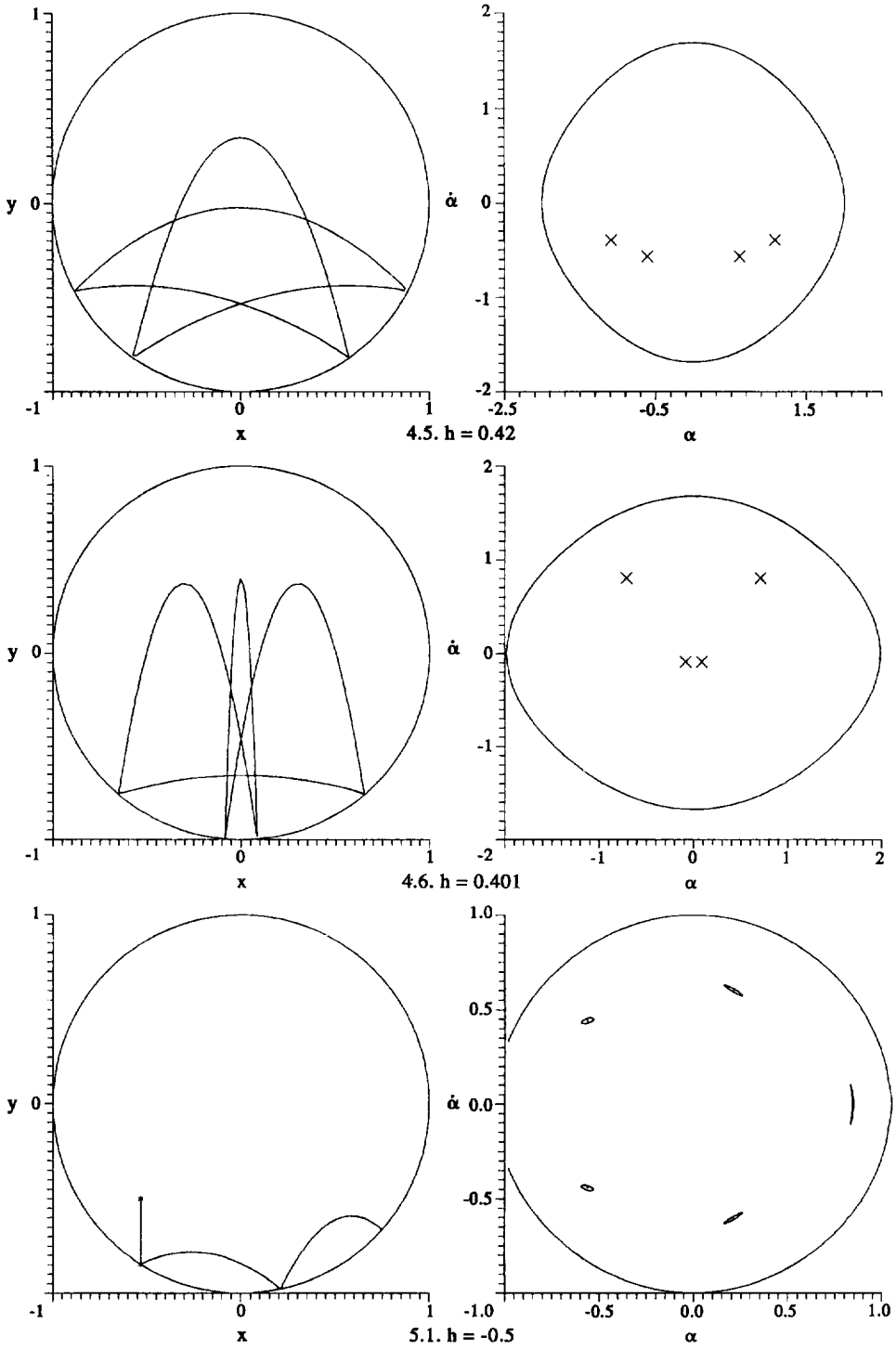

Fig. 2(e). *Caption on p. 1156.*

(f)

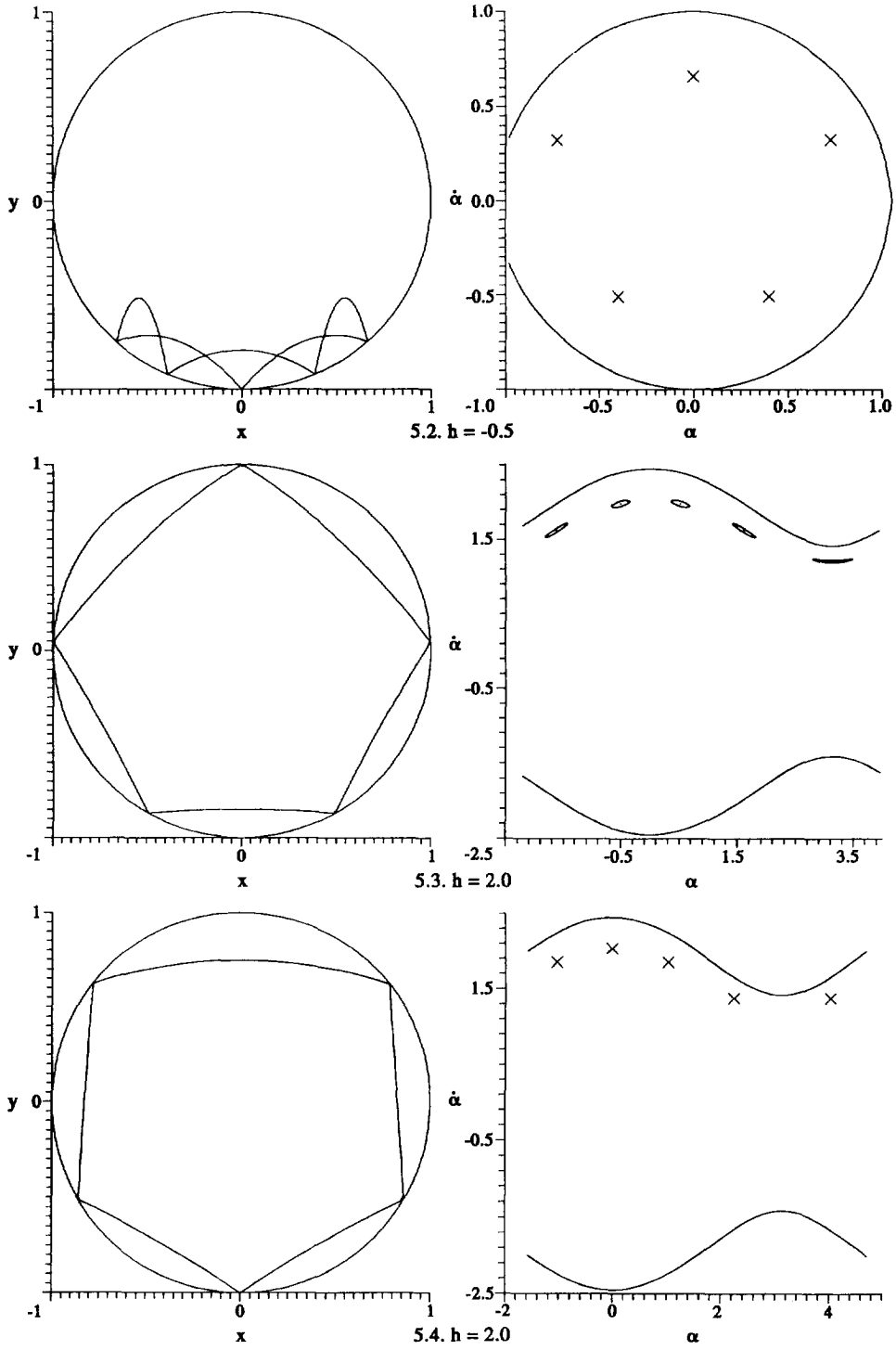

Fig. 2(f). *Caption overleaf*.

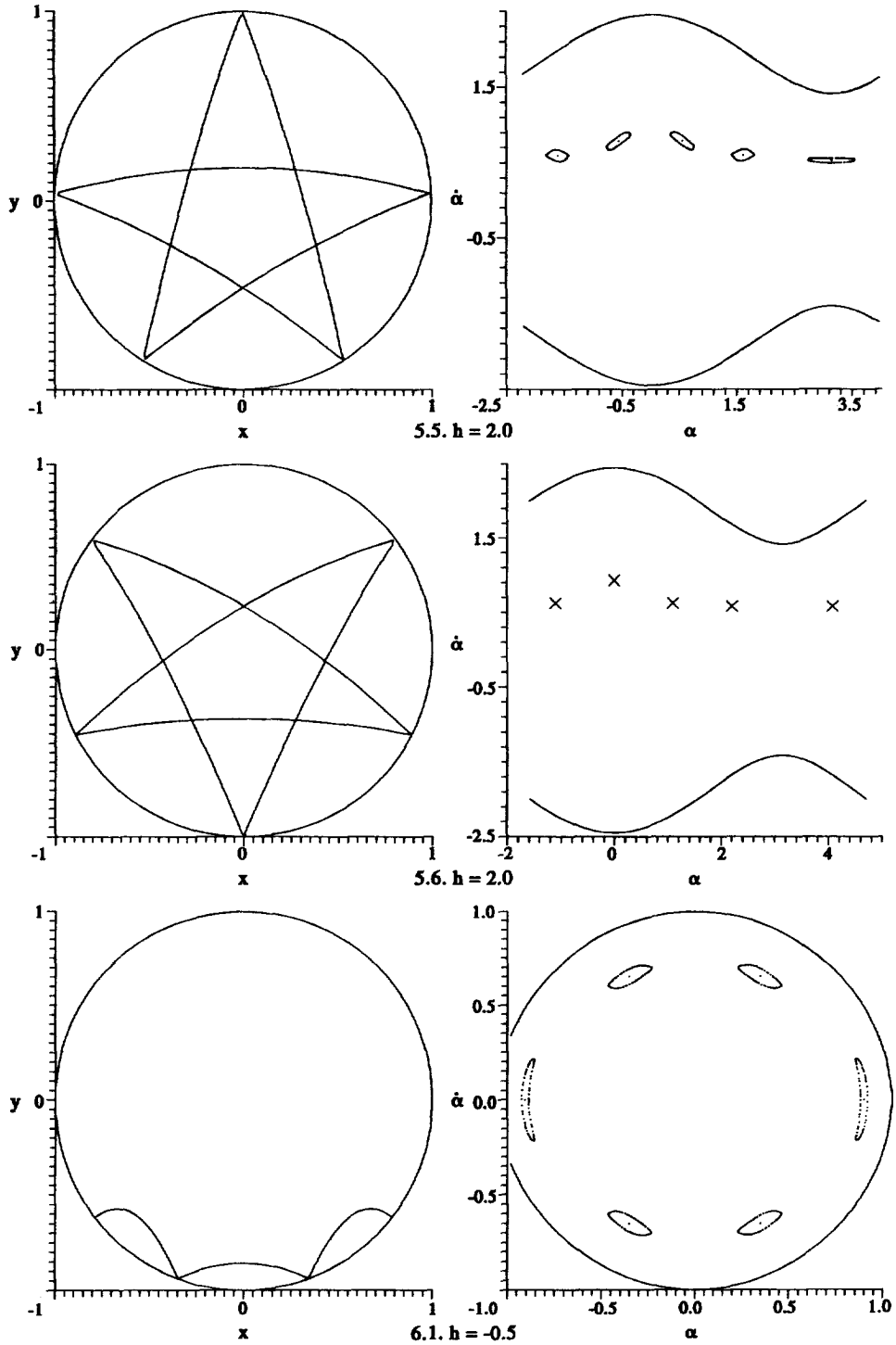

Fig. 2. (a)–(g) Periodic trajectories and their vicinities on the surface of section.

2.1. The jumps along the vertical diameter with bounces at the lowest and topmost points of the circle (2.1 in Fig. 2).

U: $u_0 = (0, 0, b_0)$, $u_1 = (\pi, 0, b_1 = \sqrt{(b_0^2 - 4)}$.

∃: $\alpha \equiv \pi$, $h > 1$.

St: In equation (10), $s = 7 - 2b_0b_1(b_0 - b_1)^2$. This implies instability for $1 < h < 1.25$ and stability to a first approximation for $h > 1.25$ [3, 4] (Fig. 1).

2.2. The motion along the parabolic arc symmetric about the vertical diameter (2.2 in Fig. 2).

U: $u_0 = (\alpha_0, 0, b_0 = \cos^{-1/2}\alpha_0)$, $u_1 = (-\alpha_0, 0, b_0)$.

∃: $0 < \alpha_0 < (\pi/2)$, $h = (2\cos\alpha_0)^{-1} - \cos\alpha_0$.

St: In equation (10), $s = 1 - 2(1 - \cos 2\alpha_0 - \cos^2 2\alpha_0)^2$. This implies stability to a first approximation for $0 < \alpha_0 < \alpha_*$ and $\alpha_* < \alpha_0 < (\pi/4)$, where $\alpha_* = \frac{1}{2}\arccos\frac{1}{2}(\sqrt{(5)} - 1)$, and instability for $(\pi/4) < \alpha_0 < (\pi/2)$; $\alpha_0 = \alpha_*$ and $\alpha_0 = (\pi/4)$ are critical cases (Fig. 1).

Δ: (a) For $\alpha_0 = \alpha_*$, $\lambda_1 = 1$, $\lambda_2 = \lambda_3 = -1$. At that α_0, the four-link *4.6* is born. For $\alpha_0 = (\pi/4)$, $\lambda_1 = \lambda_2 = \lambda_3 = 1$ and the two-link *2.3* is born at that α_0.
(b) The period of motion $T = 4\sqrt{(\cos\alpha_0)}$.

2.3. A two-link that consists of one grazing and one plunging parabola (2.3 in Fig. 2).

U: $u_0 = ((\pi/4), a_0, b_0 = (a_0^2 + \sqrt{2})^{1/2})$, $u_1 = (-(\pi/4), a_0, b_0)$.

∃: $\alpha \equiv (\pi/4)$, $0 < h < (10 - \sqrt{2})/8 \approx 1.073$.

St: In equation (10), $s = (8\sqrt{2})a_0^2 - 1$. This implies stability to a first approximation for $0 < h < \sqrt{2}/8 \approx 0.177$ and instability for $\sqrt{2}/8 < h < (10 - \sqrt{2})/8$ (Fig. 1).

Δ: $h = a_0^2$.

The motion is counter-clockwise for $a_0 > 0$ and clockwise for $a_0 < 0$. This means that the discussed family of trajectories contains two subfamilies: with direct and reverse motions.

If an angle φ_0 is introduced between the initial velocity vector $\mathbf{v}_0$ and the direction to the centre of the circle then $|\tan\varphi_0| < \frac{1}{3}$ for stable trajectories of the family under consideration. This means that the angle between the grazing and plunging segments of a stable trajectory does not exceed the value ≈37°, to the nearest degree.

3. *Three-link trajectories*

Three-link trajectories are rather difficult to analyse and we have no complete proof available that the three-link trajectory class is reduced to the families considered below. However, numerous computations of the Poincaré sections for the problem as well as the approximate analytic investigation (see Section 4) do not reveal any other three-link trajectories.

This allows us to make, with a sufficiently high degree of assurance, the following conclusion: all three-link periodic trajectories are reduced to four families *3.1*, *3.2*, *3.3*, *3.4* listed below. Numerical algorithms were mostly used to determine the existence and stability conditions for the three-link trajectories.

3.1. A nonsymmetric with respect to the vertical diameter, h-shaped periodic trajectory (3.1 in Fig. 2). The mass point moves in a segment of a vertical chord and a nonsymmetrically located parabola.

U: $u_0 = (\alpha_0, a_0, b_0)$, $u_1 = (\alpha_1, a_1, b_1)$, $u_2 = (\alpha_2 = \alpha_1, a_2 = -a_1, b_2 = b_1)$, where α_0 is the parameter. The dependence $\alpha_1(\alpha_0)$ is determined by the equation

$$(\sin\alpha_0 - \sin\alpha_1)\sin(\alpha_0 + 2\alpha_1) - 2(\cos\alpha_0 - \cos\alpha_1)\sin\alpha_0 \sin 2\alpha_1 = 0 \qquad (12)$$

and is shown in Fig. 3. The real motion inside the circle $r = 1$ corresponds to the values of α_0 within the limits $0 \leqslant \alpha_0 \leqslant 122°$ (to the nearest degree). For $\alpha_0 > 122°$, the vertical segment of the trajectory goes beyond the circle. (There exists another branch of the formal solution of equation (12), but it does not correspond to a real motion.)

Now we introduce the designations: $x_0 = \sin\alpha_0$, $y_0 = -\cos\alpha_0$, $x_1 = \sin\alpha_1$, $y_1 = -\cos\alpha_1$, $k_0 = -\cot\alpha_0$, $k_1 = -\cot\alpha_1$, $x_* = (k_1x_0 - k_0x_1)/(k_1 - k_0)$, $a_* = (k_1 - k_0)/(2(x_0 - x_1))$, $\dot{x}_0 = -(2a_*)^{-1/2}$, $\dot{y}_0 = (x_* - x_0)/\dot{x}$, $\tau = (x_1 - x_0)/\dot{x}_0$.

Then

$$a_0 = 0, \quad b_0 = -\dot{x}_0x_0 - \dot{y}_0y_0, \quad a_1 = -\dot{x}_0y_1 + (\dot{y}_0 - \tau)x_1, \quad b_1 = \dot{x}_0x_1 + (\dot{y}_0 - \tau)y_1. \qquad (13)$$

Equations (12) and (13) enable the nodes of the trajectory to be computed as functions of the natural parameter α_0.

∃: $0 < \alpha_0 < 122°(-0.625 < h < 0.989)$.

St: For $0 < \alpha_0 \leqslant 42°(-0.625 < h < -0.347)$, there is a stability to a first approximation and an instability for other values of α_0 corresponding to real motions (Fig. 1).

Δ: (a) We obtain the second subfamily of this family as mirror images of the h-shaped trajectories with respect to the vertical diameter. Each stable subfamily possesses an archipelago of three islands in the Poincaré section and both the subfamilies have a chain of six islands.

(b) The family is born from the resonant bounce 1.1 with the parameter $b_0 = \sqrt{3}/2$ ($h = -5/8 = -0.625$) and it becomes the bounce in the limit $\alpha_0 \to 0$.

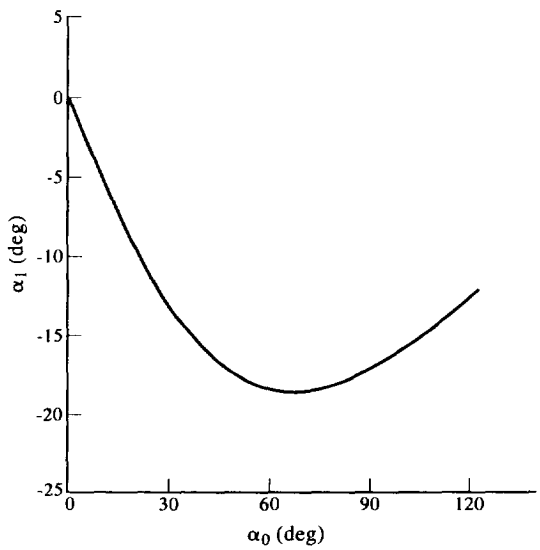

Fig. 3. The dependence α_1 (α_0) determined by equation (12) for the h-shaped periodic trajectory *3.1* in Fig. 2.

3.2. A symmetric three-link (3.2 in Fig. 2).

U: $u_0 = (\alpha_0, a_0, b_0)$, $u_1 = (-\alpha_0, a_1 = a_0, b_1 = b_0)$, $u_2 = (0, a_2, b_2)$.
We introduce an auxiliary parameter

$$\rho = \frac{2\sin\alpha_0(2 - \cos\alpha_0)}{(9 - 16\cos\alpha_0 - 16\cos^2\alpha_0 + 32\cos^3\alpha_0)^{1/2} + 2\cos^2\alpha_0 + 4\cos\alpha_0 - 3}.$$

Then $b_0 = [\sin\alpha_0/(\frac{1}{2}(1-\rho^2)\sin 2\alpha_0 + \rho\cos 2\alpha_0)]^{1/2}$, $a_0 = -\rho b_0$, $a_2 = a_0\cos\alpha_0 + b_0\sin\alpha_0$, $b_2 = a_0\sin\alpha_0 - b_0\cos\alpha_0 + (\sin\alpha_0)/a_2$.

∃: $0 < \alpha_0 < \alpha_* < (\pi/4)$ $(-0.625 < h < h_*)$, the angle α_* is determined as a root of the equation

$$F(\alpha_0) = \xi(2\eta + \xi\zeta)^2 - 8\eta = 0, \tag{14}$$

where $\zeta = \sin\alpha_0$, $\xi = -\frac{1}{2}(a_0\cos\alpha_0 + b_0\sin\alpha_0)^{-1/2}$ and

$$\eta = \sin\alpha_0(a_0\cos\alpha_0 + b_0\sin\alpha_0)^{-1/2} + \frac{a_0\sin\alpha_0 - b_0\cos\alpha_0}{a_0\cos\alpha_0 + b_0\sin\alpha_0}.$$

The numerical solution of (14) yields $\alpha_* = 41°56'10''$, $h = h_* = 0.951$. To the nearest degree, $\alpha_* = 42°$, which coincides with the stability boundary for the three-link family *3.1.*

St: All the trajectories *3.2* are unstable and $s \to -1$ as $\alpha \to 0$ and $s \to -\infty$ as $\alpha \to (\pi/4)$.

Δ: The family consists of two subfamilies with opposite directions of motion. The limiting case $\alpha = 0$ leads to the bounce *1.1* with $b_0 = \sqrt{3}/2$ $(h = -5/8 = -0.625)$, stable to a first approximation. Thus, any arbitrarily small vicinity of the resonant bounce with $b_0 = \sqrt{3}/2$ contains an unstable trajectory *3.2.*

3.3. A curvilinear triangle with one vertex at the lower point of the circle, symmetric about the vertical diameter (3.3 in Fig. 2).

U: $u_0 = (\alpha_0, a_0, b_0)$, $u_1 = (-\alpha_0, a_1 = a_0, b_1 = b_0)$, $u_2 = (0, a_2, b_2)$.
We introduce an auxiliary parameter

$$\rho = \frac{2\sin\alpha_0(2 - \cos\alpha_0)}{(9 - 16\cos\alpha_0 - 16\cos^2\alpha_0 + 32\cos^3\alpha_0)^{1/2} - 2\cos^2\alpha_0 - 4\cos\alpha_0 + 3}.$$

Then $b_0 = [\sin\alpha_0/(\frac{1}{2}(\rho^2 - 1)\sin 2\alpha_0 - \rho\cos 2\alpha_0)]^{1/2}$, $a_0 = \rho b_0$, $a_2 = a_0\cos\alpha_0 + b_0\sin\alpha_0$, $b_2 = a_0\sin\alpha_0 - b_0\cos\alpha_0 + (\sin\alpha_0)/a_2$.

∃: $(\pi/3) < \alpha_* < \alpha_0 < \frac{2}{3}\pi$, the limiting value $\alpha_0 = \alpha_*$ is a root of the equation

$$F(\alpha_0) = (a_0\sin\alpha_0 + b_0\cos\alpha_0)^2 - 2(1 + \cos\alpha_0) = 0, \tag{15}$$

the numeric solution of (15) yields $\alpha_* = 66°54'41''$.

St: To a first approximation, stability for $72°51'46'' \leqslant \alpha \leqslant 75°33'36''$ $(0.7977 \geqslant h \geqslant 0.7775)$ (Fig. 1). Instability for all other values of α_0 from the existence region.

Δ: In the limit $\alpha_0 \to \frac{2}{3}\pi$, the motion with $|\mathbf{v}| = \infty$ along an equilateral rectilinear triangle inscribed in the circle and with one vertex at its lower point.

3.4. A curvilinear triangle with one vertex at the upper point of the circle, symmetric about the vertical diameter (3.4 in Fig. 2).

U: $u_0 = (\alpha_0, a_0, b_0)$, $u_1 = (-\alpha_0, a_1 = a_0, b_1 = b_0)$, $u_2 = (0, a_2, b_2)$.
We introduce an auxiliary parameter

$$\rho = \frac{2\sin\alpha_0(2+\cos\alpha_0)}{(9+16\cos\alpha_0-16\cos^2\alpha_0-32\cos^3\alpha_0)^{1/2}-2\cos^2\alpha_0+4\cos\alpha_0+3}.$$

Then $b_0 = [\sin\alpha_0/(\frac{1}{2}(1-\rho^2)\sin 2\alpha_0 + \rho\cos 2\alpha_0)]^{1/2}$, $a_0 = -\rho b_0$, $a_2 = -a_0\cos\alpha_0 - b_0\sin\alpha_0$, $b_2 = -a_0\sin\alpha_0 + b_0\cos\alpha_0 + (\sin\alpha_0)/a_2$.

∃: $(\pi/4) < \alpha_0 < (\pi/3)$ $(1.073 \approx (10-\sqrt{(2)})/8 < h < \infty)$.

St: Stability for $(\pi/4) < \alpha_* < \alpha_0 < (\pi/3)$, $\alpha_* = 48°33'16''$ $(1.4803 < h < \infty)$. Instability for $(\pi/4) < \alpha_0 < \alpha_*$ and $s \to 1$ as $\alpha_0 \to \alpha_*$ and $s \to -1$ as $\alpha_0 \to (\pi/3)$.

Δ: The limiting case $\alpha_0 = (\pi/4)$ yields an unstable two-link 2.3, the plunging parabola which is tangent to the circle at its upper point. The limiting case $\alpha_0 = (\pi/3)$: the motion with $|\mathbf{v}| = \infty$ along an equilateral triangle with one vertex at the upper point of the circle.

4. *Four-link trajectories*

4.1. A four-link trajectory consisting of two parabolic arcs symmetric about the vertical diameter ('ticks' 4.1 in Fig. 2).

U: $u_0 = (\alpha_0,\ a_0 = 0,\ b_0 = 1/\sqrt{2})$, $u_1 = (\alpha_1 = 0,\ a_1 = -b_0\sin\alpha_0,\ b_1 = \sqrt{2} - b_0\cos\alpha_0)$, $u_2 = (\alpha_2 = -\alpha_0, a_2 = 0, b_2 = b_0)$, $u_3 = (\alpha_3 = 0, a_3 = -a_1, b_3 = b_1)$.

∃: $0 < \alpha_0 < \pi$, $h = \frac{1}{4} - \cos\alpha_0$.

St: The parameter in the characteristic equation (10) is

$$s = 1 - 2(6 - 7\cos\alpha_0 - 8\cos^2\alpha_0 + 8\cos^3\alpha_0)^2/(2-\cos\alpha_0)^2.$$

This implies: an instability for $\frac{2}{3}\pi < \alpha_0 < (\pi/2) + \arcsin((\sqrt{17}-1)/4) \approx 141°20'$, a stability, to a first approximation, for $0 < \alpha_0 < \frac{2}{3}\pi$ $(-0.75 < h < -0.25)$ and for $(\pi/2) + \arcsin((\sqrt{17}-1)/4) < \alpha_0 < \pi$ $(1.031 < h < 1.25)$ (Fig. 1).

Δ: (a) The family is born from the resonant, stable to a first approximation, bounce *1.1* with $b_0 = 1/\sqrt{2}$ $(h = -0.75)$ and transforms into it as $\alpha_0 \to 0$.

(b) As $\alpha_0 \to \pi$, the family transforms into the bounce *2.1* with the value of the parameter $b_0 = 3/\sqrt{2}$ $(h = 1.25)$, which is on the boundary between stable and unstable bounces *2.1*.

(c) The family is isochronal: all the trajectories have the same initial velocity $v = 1/\sqrt{2}$ and the same period $T = 4/\sqrt{2}$.

4.2. A four-link w-shaped trajectory consisting of a parabolic arc symmetric about the vertical diameter and two vertical chord segments of the same height (4.1 in Fig. 2).

U: $u_0 = (\alpha_0, a_0, b_0)$, $u_1 = (\alpha_0, a_1 = -a_0, b_1 = b_0)$, $u_2 = (-\alpha_0, a_2 = -a_0, b_2 = b_0)$, $u_3 = (-\alpha_0, a_3 = a_0, b_3 = b_0)$, $a_0 = \sin\alpha_0(2\cos\alpha_0\cos 2\alpha_0)^{-1/2}$, $b_0 = \cos\alpha_0(2\cos\alpha_0\cos 2\alpha_0)^{-1/2}$.

∃: $0 < \alpha_0 < \alpha_* < (\pi/4)$, $\alpha_* = \arccos[\frac{1}{2}(\frac{1}{2} + (1/\sqrt{2}))]^{1/2} \approx 39°01'$, $h = 1/(4\cos\alpha\cos 2\alpha_0) - \cos\alpha_0$.

St: All the trajectories *4.2* are unstable and $s \to -1$ as $\alpha_0 \to 0$ (and $s \to -\infty$ as $\alpha_0 \to (\pi/4)$).

Δ: The limiting case $\alpha_0 = 0$ yields the bounce *1.1* with $b_0 = 1/\sqrt{2}$. The trajectories *4.2* are born together with *4.1* from this resonant bounce.

4.3. A curvilinear quadrangle with vertices at the lower and upper points of the circle, symmetric about the vertical diameter (4.3 in Fig. 2). Periodic solutions of this family exist and they are stable for all sufficiently large values of the energy constant $h > h_* \approx 1.621$.

The value $h = h_*$ is bifurcational (the period-doubling bifurcation). For $h < h_*$, the discussed four-link trajectories are unstable, but stable symmetric eight-link trajectories, close to the four-link ones, come into being. These eight-link trajectories have a rather small region of stability.

A more detailed information about the family *4.3* is as follows:

U: $u_0 = (\alpha_0, a_0, b_0)$, $u_1 = (\alpha_1 = \pi, a_1, b_1)$, $u_2 = (\alpha_2 = -\alpha_0, a_2 = a_0, b_2 = b_0)$, $u_3 = (\alpha_3 = 0, a_3, b_3)$,

$$a_0 = \frac{\sin\alpha_0}{[2\cos\alpha_0(1 - 4\cos^2\alpha_0)^{1/2}]^{1/2}}, \qquad b_0 = \frac{1 + (1 - 4\cos^2\alpha_0)^{1/2}}{[8\cos\alpha_0(1 - 4\cos^2\alpha_0)^{1/2}]^{1/2}},$$

$a_1 = -a_0\cos\alpha_0 + b_0\sin\alpha_0$, $a_3 = a_0\cos\alpha_0 + b_0\sin\alpha_0$, $b_1 = a_0\sin\alpha_0 + b_0\cos\alpha_0 - (\sin\alpha_0)/a_1$, $b_3 = a_0\sin\alpha_0 - b_0\cos\alpha_0 + (\sin\alpha_0)/a_3$.

∃: $\alpha_* < \alpha_0 < (\pi/2)$ $(1.152 < h < \infty)$, $\alpha_* \approx 66°55'$.

St: $\alpha_* < \alpha_0 \leq 73°48'$ $(1.152 < h < 1.621)$—instability.
$73°49' \leq \alpha_0 < 90°$ $(1.621 \leq h < \infty)$—stability.

Δ: For $\alpha_0 = \alpha_*$, the four-link *4.3* transforms into the three-link *3.3* with tangency at the upper point of the circle $(b_1 = 0)$.

4.4. A curvilinear quadrangle with vertices that are pairwise symmetric about the vertical diameter (4.4 in Fig. 2).

U: The nodes $u_0 = (\alpha_0, a_0, b_0)$, $u_1 = (\alpha_1, a_1, b_1)$, ... cannot be expressed by simple formulas.

∃: $25°38' < \alpha_0 < 45°$ ($80°21' < \alpha_1 < 135°$, respectively). The dependence $h(\alpha_1)$ is shown in Fig. 1.

St: Stable for $27°22' < \alpha_0 < 27°57'$ ($86°43' < \alpha_1 < 88°50'$), i.e. for $1.038 < h < 1.045$, and unstable in the rest of the existence region.

Δ: For $\alpha_0 = 45°$ $(\alpha_1 = 135°)$—motion along an inscribed square with infinite speed (the Birkhoff billiard).

4.5. An exotic self-intersecting four-link (4.5 in Fig. 2).

∃: $29°29' < \alpha_0 < 45°$, respectively, $45° < \alpha_2 < 80°40'$ $(0.177 \approx \sqrt{2}/8 < h < 1.032)$. Both the dependences $h(\alpha_0)$ and $h(\alpha_2)$ are shown in Fig. 1.

St: Stable for $41°22' < \alpha_0 < 45°$, respectively, $45° < \alpha_2 < 49°22'$ $(\sqrt{2}/8 < h < 0.2)$. Unstable in the rest of the existence region.

Δ: For $\alpha_0 = 45°$, it transforms into the two-link *2.3* on the boundary between regions of stable and unstable trajectories 2.3.

4.6. An exotic self-intersecting four-link (4.6 in Fig. 2).

∃: $3°12' < \alpha_0 < \alpha_* = \frac{1}{2}\arccos(\sqrt{5} - 1)/2 \approx 25°55'$, respectively, $\alpha_* < \alpha_2 < 42°04'$ $(-0.34 < h < -0.95)$. Both the dependences $h(\alpha_0)$ and $h(\alpha_2)$ are shown in Fig. 1.

St: Stability for $16°3' < \alpha_0 < \alpha_*$, respectively, $\alpha_* < \alpha_2 < 33°33'$ $(-0.34 < h < -0.28)$.

Δ: For $\alpha_0 = \alpha_*$, it transforms into the resonant case of the two-link *2.2*.

5. *Five-link trajectories*

Five-link trajectories have not been studied closely. However, extensive numerical computations have revealed the following five-link trajectories presented in Fig. 2:

5.1. Nonsymmetric m-shaped trajectories with two parabolic arcs (chord–arc–arc). They exist and are stable for some negative values of the energy h.

5.2. Trajectories consisting of three symmetrically placed arcs and two more arcs, also symmetric. They exist for some $h < 0$ and are unstable.

5.3. Pentagons with a vertex at the upper point of the circle. They exist and are stable for some sufficiently large positive h.

5.4. Pentagons with a vertex at the lower point of the circle. They exist for sufficiently large $h > 0$ and are unstable.

5.5. Five-pointed stars with a vertex at the upper point of the circle. They exist and are stable for sufficiently large $h > 0$.

5.6. Five-pointed stars with a vertex at the lower point of the circle. They exist for sufficiently large $h > 0$ and are unstable.

6. *Six-link trajectories*

Of six-link trajectories we distinguish the family:

6.1. This family of trajectories consist of three arcs placed symmetrically about the vertical diameter (6.1 in Fig. 2). These six-links significantly affect the phase portrait of the problem. The curve $h(\alpha)$ for this six-link is presented in Fig. 1. The stability interval is $0 < \alpha < 62°$. However, for $\alpha \approx 53°17'$, the stability parameter $s = 1$, and this corresponds to the critical case and bifurcation (families of stable and unstable twelve-links are born).

4. ON THE SYMMETRY OF PERIODIC TRAJECTORIES

As $h \to \infty$, the gravitational billiard considered approaches the Birkhoff billiard in a circle. The latter allows for a continuum of periodic trajectories. Each of them may be rotated as a whole through an arbitrary angle around the centre of the circle giving birth to a new periodic trajectory. However, this property does not hold when a weak gravitational field is switched on (which is equivalent to the case of rather large values of h for a field of a limited force). Numerical experiments show the presence of only periodic trajectories symmetric about the vertical diameter of the circle. This is also true for low energy levels except for h-shaped trajectories with various numbers of links. No other nonsymmetrical periodic trajectories have been found. Thus we can say that the gravity field acts selectively eliminating nonsymmetrical periodic trajectories. We shall now examine this phenomenon.

In a weak gravitational field g, take $\varepsilon = -\frac{1}{2}g$, $|\varepsilon| \ll 1$. One link of a trajectory is described by the equation

$$y + \cos\alpha_0 = \varepsilon(x - \sin\alpha_0)^2 - \cot(\alpha_0 + \varphi_0)(x - \sin\alpha_0), \tag{16}$$

where α_0 is an angular coordinate of the collision point, and φ_0 is the reflection angle, $-\pi/2 < \varphi_0 < \pi/2$.

For the Birkhoff billiard, $\varepsilon = 0$ and a trajectory link is a segment of a straight line. The reflection angle φ is an invariant and the mapping of the phase cylinder boundary is given by the formulas

$$\alpha_{n+1} = \alpha_n + 2\varphi_n - \pi, \qquad \varphi_{n+1} = \varphi_n, \qquad n = 0, 1, 2, \ldots. \tag{17}$$

A necessary and sufficient condition of a trajectory periodicity is the commensurability of the invariant $\varphi \equiv \varphi_0$ with π, namely:

$$\varphi = (p/2q)\pi, \qquad p - q = 2k, \qquad |p| < |q|, \qquad p, q, k \in \mathbb{Z}. \tag{18}$$

In a weak gravitational field ($|\varepsilon| \ll 1$), we search for the mapping $(\alpha_0, \varphi_0) \to (\alpha_1, \varphi_1)$ in the form

$$\alpha_1 = \alpha_0 + 2\varphi_0 - \pi + \varepsilon\delta_1 + \varepsilon^2\beta_1 + \mathbb{O}(\varepsilon^3), \qquad \varphi_1 = \varphi_0 + \varepsilon\gamma_1 + \varepsilon^2\chi_1 + \mathbb{O}(\varepsilon^3).$$

By using (16) and the equation for the angle of incidence

$$\left.\frac{dy}{dx}\right|_{x=x_1} = -\cot(\alpha_1 - \varphi_1),$$

we obtain

$$\begin{aligned}
\delta_1 &= -4\cos\varphi_0 \sin^3(\alpha_0 + \varphi_0),\\
\beta_1 &= 8\cos\varphi_0 \sin^5(\alpha_0 + \varphi_0)[2\cos(\alpha_0 + \varphi_0)\cos\varphi_0 - \sin\varphi_0 \sin(\alpha_0 + \varphi_0)],\\
\gamma_1 &= 0,\\
\chi_1 &= -4\cos^2\varphi_0 \sin^4(\alpha_0 + \varphi_0)\sin 2(\alpha_0 + \varphi_0).
\end{aligned} \tag{19}$$

In a similar way, by constructing the mapping $(\alpha_1, \varphi_1) \to (\alpha_2, \varphi_2)$, and so on, we have after q mappings

$$\alpha_q = \alpha_0 + 2q\varphi_0 - q\pi + \varepsilon\sum_{i=1}^{q}\delta_i + \varepsilon^2\sum_{i=1}^{q}(\beta_i + 2(q-i)\chi_i) + q^2\mathbb{O}(\varepsilon^3),$$

$$\varphi_q = \varphi_0 + \varepsilon^2\sum_{i=1}^{q}\chi_i + q\mathbb{O}(\varepsilon^3).$$

We search for φ_0 of a periodic trajectory in the gravitating billiard in the form

$$\varphi_0 = \varphi + \varepsilon\varphi_{01} + \varepsilon^2\varphi_{02} + \mathbb{O}(\varepsilon^3), \tag{20}$$

where φ is determined by the trajectory periodicity conditions (18) for the Birkhoff billiard. The periodicity conditions for the gravitating billiard are as follows:

$$\alpha_q = \alpha_0 + 2\pi k, \qquad \varphi_q = \varphi_0. \tag{21}$$

The first equation of (21), in view of (20), implies

$$\varphi_{01} = -\frac{1}{2q}\sum_{i=1}^{q}\delta_i, \qquad \varphi_{02} = -\frac{1}{2q}\sum_{i=1}^{q}(\beta_i + 2(q-i)\chi_i).$$

The second equation of (21) yields the only necessary condition of periodicity:

$$\sum_{i=1}^{q}\chi_i = 0. \tag{22}$$

After replacing the index 1 by i, and 0 by $i-1$ in the last equation of (19), insert the expression for χ_i into (22). Also substitute the initial approximations for α_{i-1}, φ_{i-1} from the theory of the Birkhoff billiard according to equations (17) and (18). Then, we obtain (22) in the expanded form:

$$4\cos^2\left(\frac{\pi}{2}\frac{p}{q}\right)\sum_{i=0}^{q-1}\sin^4\left(\alpha_0 + \frac{\pi}{2}\frac{p}{q} + i\pi\frac{p}{q}\right)\sin\left(2\alpha_0 + \pi\frac{p}{q} + 2i\pi\frac{p}{q}\right) = 0, \tag{23}$$

which is equivalent to the condition

$$\sum_{i=0}^{q-1}\left[\tfrac{5}{4}\sin\left(c + 2i\pi\frac{p}{q}\right) - \sin\left(2c + 4i\pi\frac{p}{q}\right) + \tfrac{1}{4}\sin\left(3c + 6i\pi\frac{p}{q}\right)\right] = 0, \tag{24}$$

where $c = 2\alpha_0 + \pi p/q$.

It can be shown that

$$\sum_{i=0}^{q-1} \sin 2\pi i\frac{m}{q} = 0, \qquad m \in \mathbb{Z}, \tag{25}$$

and

$$\sum_{i=0}^{q-1} \cos 2\pi i\frac{m}{q} = \begin{cases} q, \text{ if } m/q = j, \\ 0, \text{ if } m/q \neq j. \end{cases} \qquad m, j \in \mathbb{Z}, \tag{26}$$

By developing the sines of the sums in (24) and taking into account equations (25) and (26), we find that (24) is always met identically for any c, except in the following essentially different cases:

$$\text{I. } p = 0,\ q = 2. \quad \text{II. } p = \pm 1,\ q = 3. \quad \text{III. } p = \pm 2,\ q = 4. \quad \text{IV. } p = \pm 4,\ q = 6. \tag{27}$$

The negative values of p correspond to time-reversed motion. We shall now consider these cases.

I. $p = 0$, $q = 2$. The unperturbed trajectory is a diameter of the circle. Inserting the values of p, q in (23) yields $\sin^4\alpha_0 \sin 2\alpha_0 = 0$ and so $\alpha_0 = (\pi/2)n$, $n \in \mathbb{Z}$. Thus, among all possible two-link trajectories, the gravity selects only two symmetric trajectories, which are born from the vertical and horizontal diameters (recalling that we are dealing with a weak field).

II. $p = \pm 1$, $q = 3$. The unperturbed trajectory is an equilateral triangle. Inserting the values of p, q in (24) yields $\sin 6\alpha_0 = 0$ and so $\alpha_0 = (\pi/6)n$, $n \in \mathbb{Z}$. Only triangles, one vertex of which lies at the lower or upper point of the circle (the first group) or at the intersection of the horizontal diameter with the circle (the second group), are selected. The numerical experiment revealed similar three-link trajectories from the first group only. These trajectories are symmetric about the vertical diameter. Recall that the condition (23) (or (24)) is merely the necessary condition for periodicity of a trajectory.

III. $p = \pm 2$, $q = 4$. Squares in the unperturbed motion. Equation (24) yields $\sin 4\alpha_0 = 0$ and so $\alpha_0 = (\pi/4)n$, $n \in \mathbb{Z}$. These are generating trajectories—either squares with vertices at the intersections of the horizontal and vertical diameters with the circle (the first group) or squares with horizontal and vertical sides (the second group). The numerical computation discovered the trajectories of both the groups.

IV. $p = \pm 4$, $q = 6$. Regular hexagons in the unperturbed motion. Equation (24) yields $\sin 6\alpha_0 = 0$ and so $\alpha_0 = (\pi/6)n$, $n \in \mathbb{Z}$. This condition selects two groups of hexagons: those with a pair of vertical sides (the first group) and those with a pair of horizontal sides (the

second group). The trajectories belonging to either group were found during the numerical computation.

Thus, we have shown that imposing the weak gravitational field leads to the disappearance of nonsymmetric two-, three-, four-, and six-link trajectories. The five-link trajectories are not covered by the theory in the approximation considered and they remain arbitrarily orientated. It seems likely that the selection of the five-links as well as the trajectories having seven and more links may be carried out by taking into account the expansion terms of higher powers of ε.

The theory developed can be called quasi-linear in the sense that the trajectories under study consist of near-straight links. In the essentially non-linear cases, it is also sometimes possible to demonstrate the selective properties of the gravitational field (the selection of symmetrical trajectories).

We will show this by the example of the two-link trajectories *2.2*—the motion back and forth along the parabolic arc. Denote the angular deviations of the points of the collision with the circle from the vertical downwards direction by α and $-\beta$, $\alpha > 0$, $\beta > 0$. For the existence of such a trajectory, it is necessary to put $a_0 = a_1 = 0$ in Equations (6) to (8). Then, it follows from these equations that

$$b_1 \sin\beta = b_0 \sin\alpha, \qquad -\tfrac{1}{2}b_1^2 \sin 2\beta + \sin\beta = \tfrac{1}{2}b_0^2 \sin 2\alpha - \sin\alpha,$$
$$\tfrac{1}{2}b_1^2 - \cos\beta = \tfrac{1}{2}b_0^2 - \cos\alpha. \tag{28}$$

This implies the existence of the symmetric trajectory *2.2*:

$$\alpha = \beta, \qquad b_1 = b_0 = (\cos\alpha)^{-1/2}.$$

We seek for the nonsymmetric trajectory

$$\alpha \neq \beta, \qquad \pi > \alpha > 0, \qquad \pi > \beta > 0, \qquad b_0 > 0, \qquad b_1 > 0.$$

Resolving the first and third equations of (28) with respect to b_0, b_1, we have

$$b_0^2 \cos\frac{\alpha+\beta}{2}\cos\frac{\alpha-\beta}{2} = \sin^2\beta, \qquad b_1^2 \cos\frac{\alpha+\beta}{2}\cos\frac{\alpha-\beta}{2} = \sin^2\alpha.$$

Substituting the expressions for b_0^2 and b_1^2, obtained from the equations above, into the second equation of (28), we bring this equation to the form:

$$[1 + \cos(\alpha+\beta)]\frac{\sin((\alpha+\beta)/2)}{\cos((\alpha-\beta)/2)} = 0,$$

which cannot be satisfied because of the essential positiveness of the left-hand side. The desired non-symmetric trajectories do not exist.

Note that the principle of the symmetry of the periodic trajectories derives from the superposition of the two factors: the gravitation and the perfect symmetry of the circular billiard. For example, the elliptic gravitating billiard with the boundary $x = A\sin\alpha$, $y = -\cos\alpha$, $0 < A < 1$, allows for the non-symmetric two-link trajectory with the nodes

$$\alpha_0 = \frac{\pi}{2}, \qquad a_0 = 0, \qquad b_0 = \frac{A}{\sqrt{(2-A^2)}\sqrt[4]{(1-A^2)}},$$
$$\alpha_1 = -\arcsin\left(\frac{A^2}{2-A^2}\right), \qquad a_1 = 0, \qquad b_1 = \frac{\sqrt{(4-3A^2)}}{\sqrt{(2-A^2)}\sqrt[4]{(1-A^2)}}.$$

5. THE POINCARÉ SURFACES OF SECTION

The performed analysis of the existence and stability of the periodic trajectory families makes it possible to represent the main features of the phase portrait for a fixed energy level. This is carried out by accumulation of 'archipelagos' that correspond to the particular stable periodic motions existing on a given energy level. Then the numerical implementation of the Poincaré mapping is used, which enables us to describe surfaces of section in more detail, including chaotic seas and archipelagos of regular motions.

We now turn our attention to Fig. 1. The region of the parameters definition in the plane (α, h) is $h > -\cos\alpha$. The boundary of this region is marked in Fig. 1. A fixed energy level h_0 is corresponded in the phase plane $(\alpha, \dot{\alpha})$ by the motion existence region defined by the inequality $\frac{1}{2}\dot{\alpha}^2 - \cos\alpha \leq h_0$. On the boundary $\frac{1}{2}\dot{\alpha}^2 - \cos\alpha = h_0$ of this region, depending on the value h_0, there is either a continuous pendulum-like motion on the constraint $r = 1$ or a motion on this constraint until the moment of leaving it (see Section 6).

Now we describe the Poincaré surfaces of section and their main features for various energy levels.

1. $-1.0 < h \leq -0.75$. It is clear from Fig. 1 that, for this interval of the energy values, among stable periodic trajectories with a rather small number of links, there exist only stable vertical bounces *1.1* at the lower point of the circle. They correspond to the stable origin (centre) on the Poincaré phase plane. The absence of other periodic motions in the vicinity of the origin provides a high degree of regularity (a rather small stochasticity). Indeed, the Poincaré section is shown in Fig. 4 for $h = -0.75$, where one can clearly see all that has been noticed above. Only closer to the boundary are located the archipelagos of 6

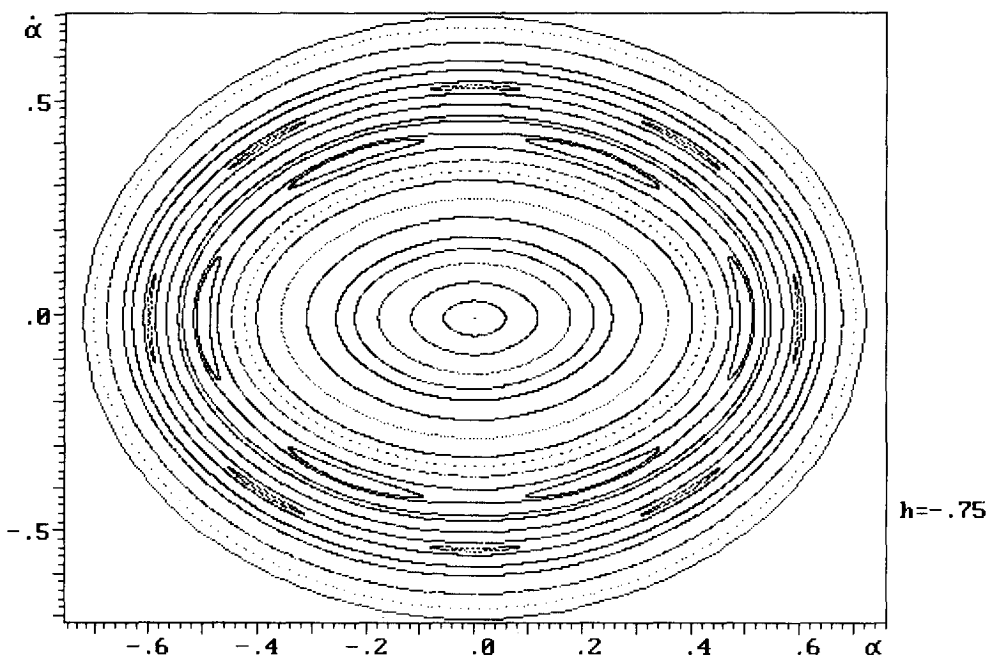

Fig. 4. Surface of section for $h = -0.75$. The stable origin (centre) corresponds to stable vertical bounces *1.1* at the lower point of the circle. Weak stochasticity.

and 8 islands, the centres of which correspond to the six- and eight-link stable periodic motions. (These are of oscillatory type: with change of the sign of $\dot{\alpha}$, the motions proceed back and forth along the chain of the parabolic arcs.)

2. $-0.75 < h \leqslant -0.625$. The preceding picture is superimposed by the four-link archipelago, which corresponds to the four-link periodic trajectory *4.1*. This archipelago is located closer to the origin than the six-island one; the stochasticity makes itself evident (Fig. 5).

3. $-0.625 < h \leqslant -0.5$. It is clear from Fig. 1 that, on these energy levels, the Poincaré section is characterized, as one increases the distance from the origin, by the islands that correspond to the motions *1.1*, *3.1* and *4.1*. The archipelago associated with the three-link trajectories consists of a pair of symmetrically located three-island archipelagos. The stochasticity is already quite significant. The Poincaré plane contains, apart from the above-listed archipelagos, a number of multi-link ones including a six-link chain that consists of rather large islands (lying nearer to the boundary of the possible motion region). One can see in Fig. 6 that all this is also typical for the limiting energy level ($h = -0.5$). Here, the islands of the three-link archipelagos are of significantly smaller sizes than those of the six-link.

4. $-0.5 < h \leqslant -0.347$. It is obvious from Fig. 1 that there exists no island with its centre at the origin (the vertical bounce is unstable). An archipelago of two islands (the two-link *2.2*) evolved from it as a result of the bifurcation. Further, as one increases the distance from the origin, there are three-links *3.1* and four-links *4.1*. The islands are decreasing in size, the stochasticity is growing. This situation is shown in Fig. 7 for $h = -0.4$.

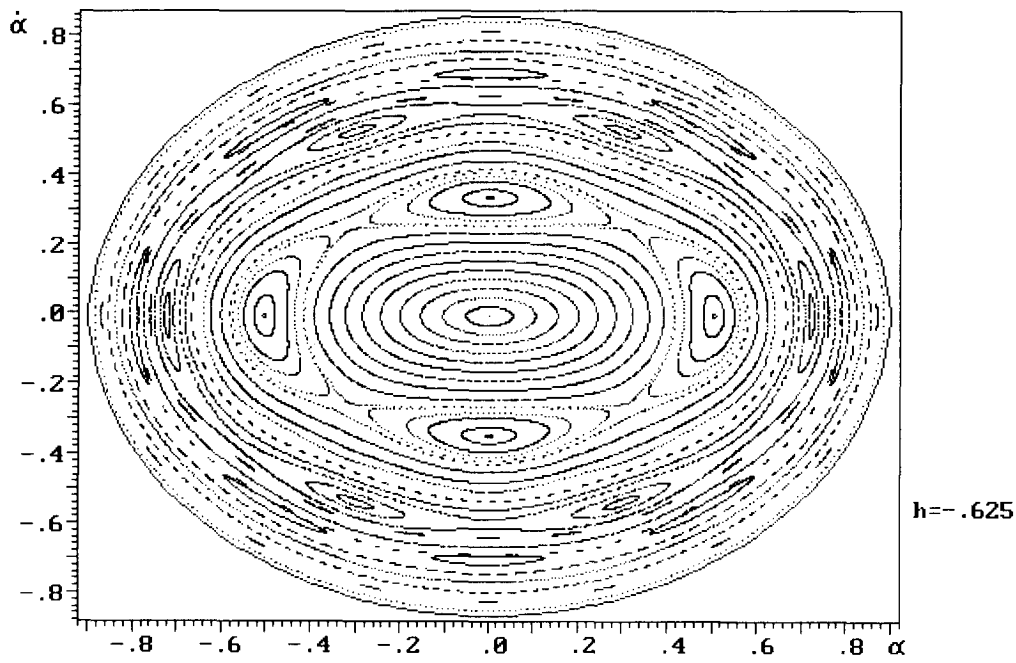

Fig. 5. Surface of section for $h = -0.625$. A four-link archipelago arises that corresponds to trajectory *4.1*.

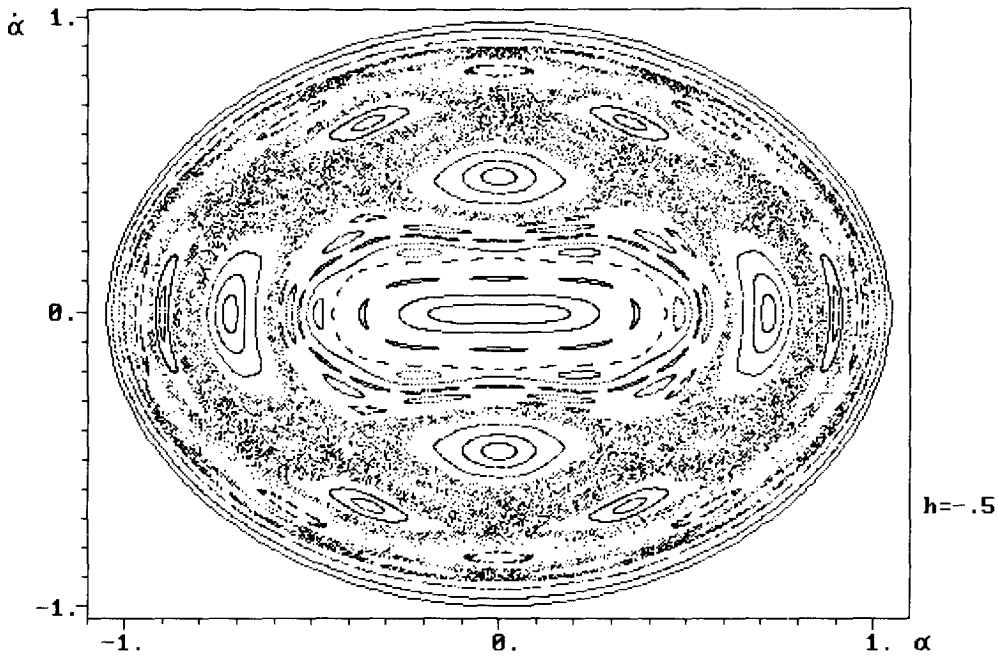

Fig. 6. Surface of section for $h = -0.5$. Stochasticity develops. There are a number of multi-link chains of islands.

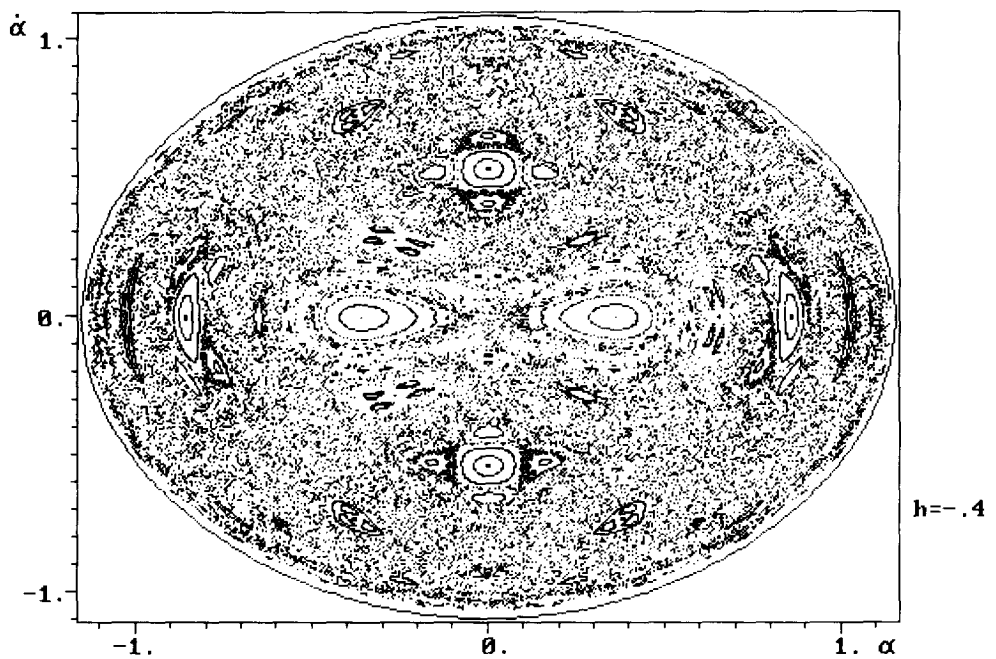

Fig. 7. Surface of section for $h = -0.4$. There is no island with its centre at the origin (the vertical bounce is unstable). A chain of two islands (the two-link *2.2*) evolves from it as a result of the bifurcation. Other islands decrease in size.

5. $-0.347 < h \leq -0.25$. The stable three-links disappear. The families *2.2* and *4.1* remain. In Fig. 8 for $h = -0.25$, the family *4.1* is on the verge of the bifurcational disappearance. In Fig. 8 one can see virtually no other archipelagos, which are flooded with the chaotic sea.

6. $-0.25 < h \leq 0$. The numerical implementation of the Poincaré mapping revealed strong stochasticity. According to Fig. 1, the islands must remain that correspond to the two-link *2.2*. In Fig. 9 ($h = 0$), these islands are on the verge of the bifurcation—the transformation into a pair of two-island archipelagos, associated with the family *2.3*.

The value $\lambda_{\max}$ of the maximal Lyapunov exponent may serve as a measure of stochasticity. For regular motions $\lambda_{\max} = 0$ and $\lambda_{\max}$ grows as the motion increases stochasticity.

Presented in Fig. 10 are the results of $\lambda_{\max}$ evaluation as a function of the number of collisions for the energy level $h = 0$. The precise value of $\lambda_{\max}$ is determined as a limit as $n \to \infty$ [5]. A rapid convergence $\lambda_{\max} \to 0$ is observed along a regular trajectory $\lambda_{\max} \to 0$. Two computation variants are presented with different initial conditions. For both of them, the convergence to the limiting value $\lambda_{\max} \approx 0.591$ is seen, which corresponds to the significant stochasticity.

7. $0 < h \leq 0.175$. A pair of two-island archipelagos in the chaotic sea, they are associated with the two-links 2.3 with the motion of the rotatory type (the angular velocity does not change its sign; see Fig. 11 in which $h = 0.1$). The islands are quite small and it is hard to detect them in the chaotic sea.

8. $0.175 < h \leq 1.031$. There is a global chaos, and a pair of three-island archipelagos arise only in the very small subregion of the parameter values that correspond to the family *3.3*.

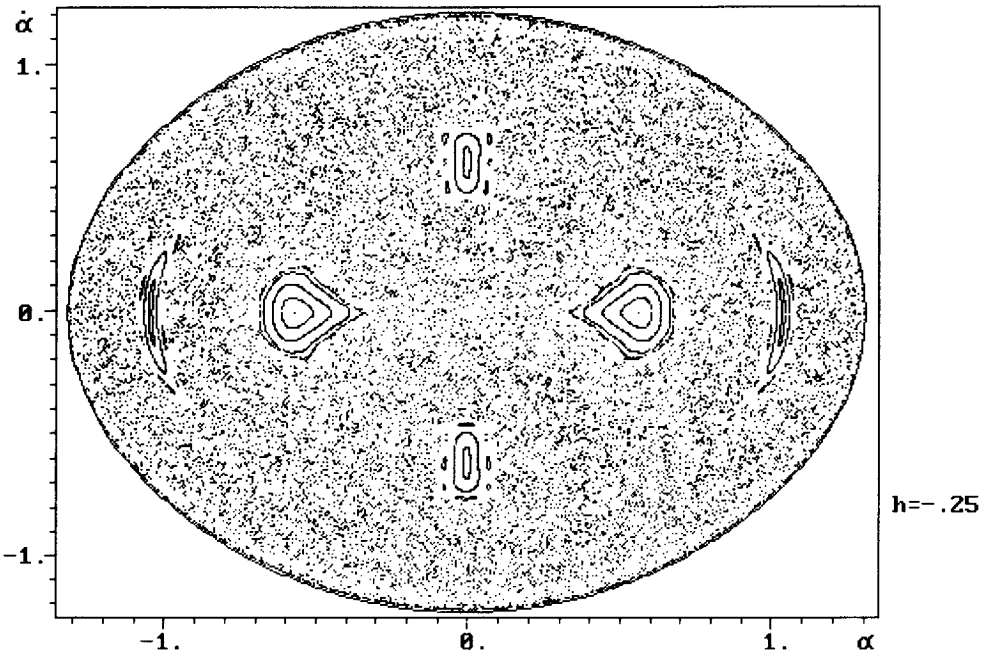

Fig. 8. Surface of section for $h = -0.25$. The stable three-links disappear. The families *2.2* and *4.1* remain. The family *4.1* is on the verge of bifurcational disappearance.

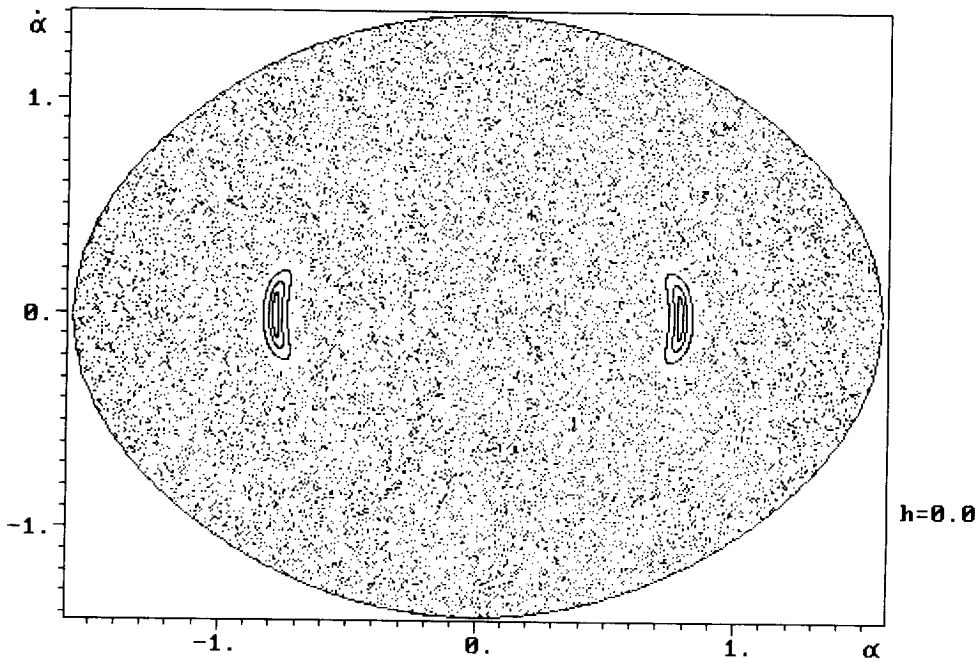

Fig. 9. Surface of section for $h = 0$. Strong stochasticity. The two-link *2.2* islands are about to bifurcate into a pair of two-island archipelagos associated with the family *2.3*.

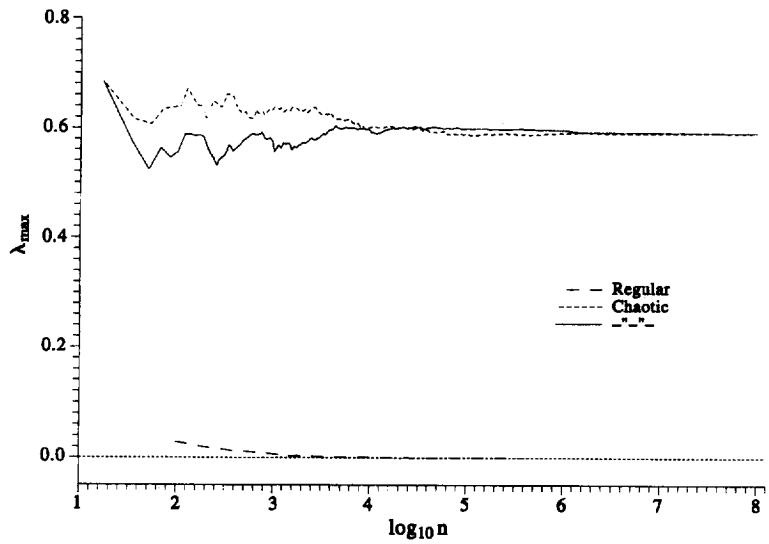

Fig. 10. Convergence of the maximal Lyapunov exponent for the energy level $h = 0$ and for different initial conditions.

The islands are quite small and it is hard to detect them in the chaotic sea (Fig. 12, $h = 0.78$).

9. $1.031 < h \leq 1.25$. In the chaotic sea the gaps come into view. There is an archipelago corresponding to the family *4.1* (Fig. 13).

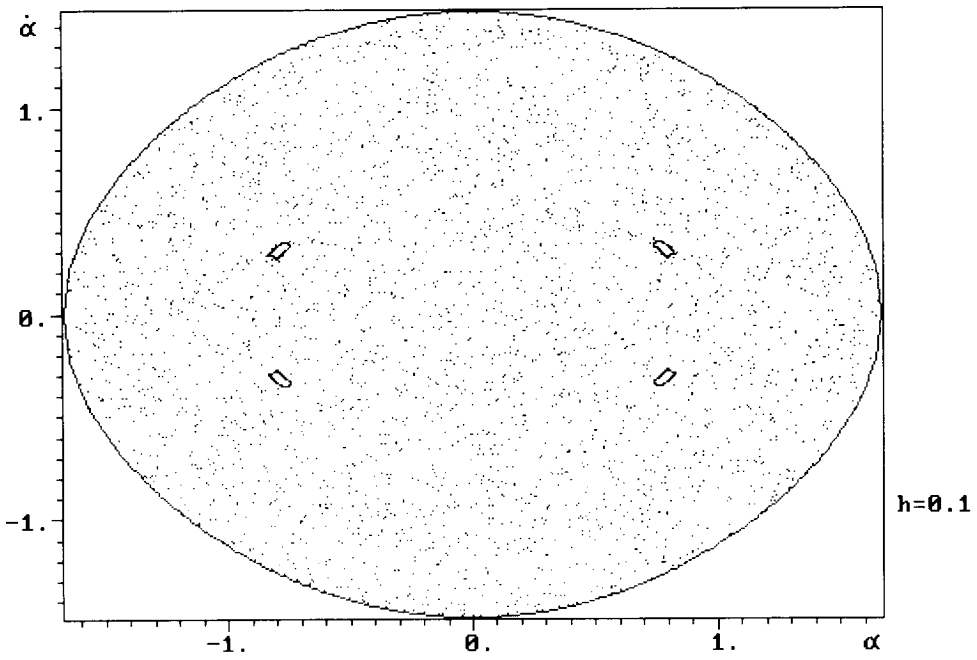

Fig. 11. Surface of section for $h = 0.1$. A pair of small two-island archipelagos in the chaotic sea. They are associated with the two-links *2.3* with motion of the rotatory type.

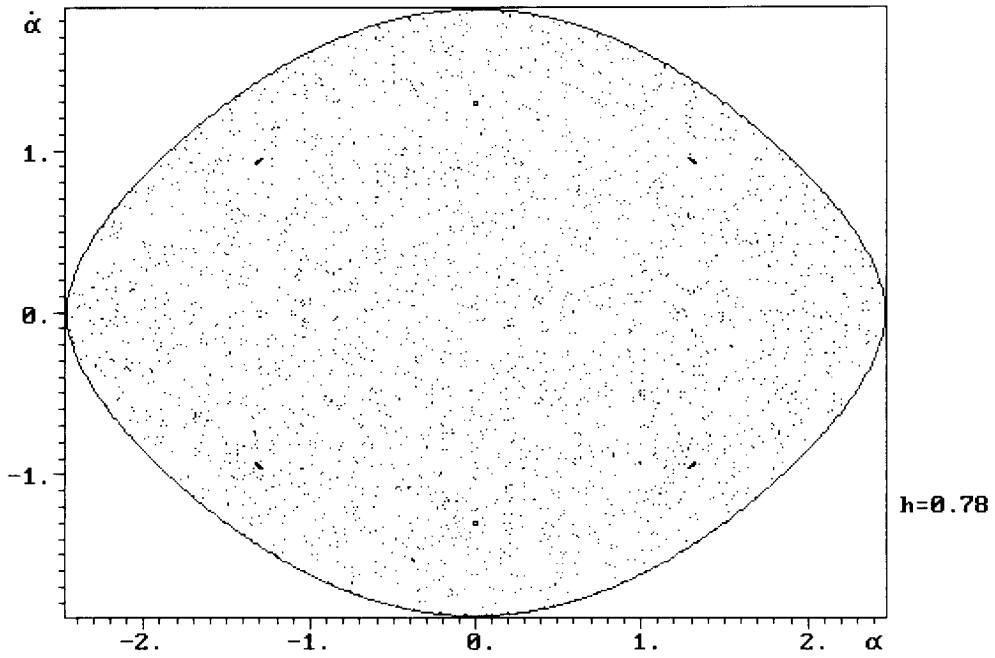

Fig. 12. Surface of section for $h = 0.78$. Global chaos. A pair of tiny three-island archipelagos correspond to the family *3.3*.

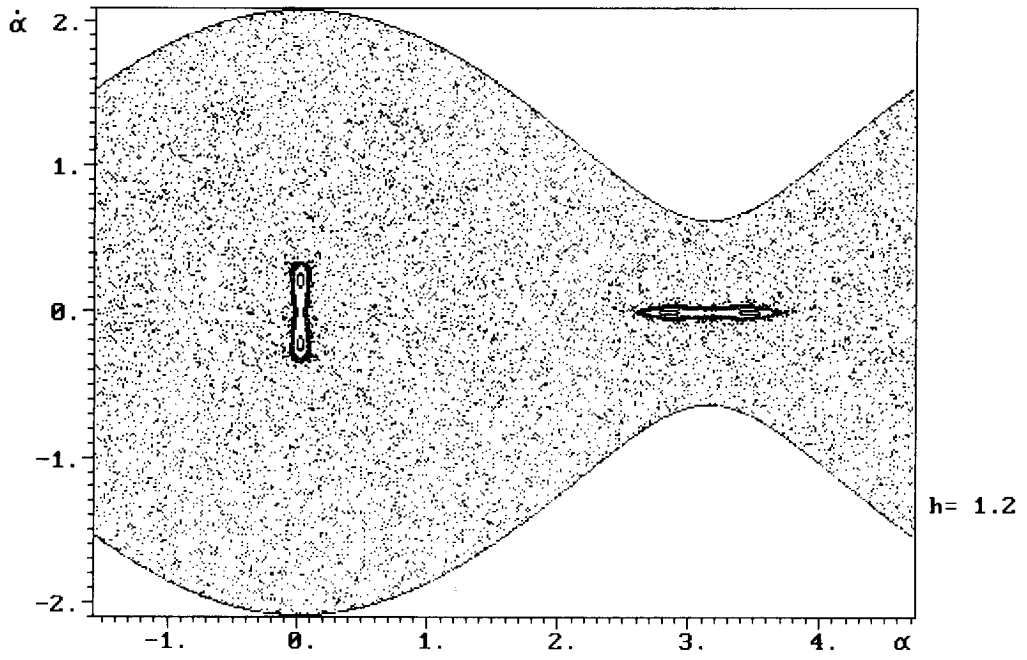

Fig. 13. Surface of section for $h = 1.2$. In the chaotic sea the gaps come into view. There is a chain corresponding to the family *4.1*.

10. $1.25 < h \leqslant 1.48$. The family *4.1* transforms into 2.1 (Fig. 14).

11. $1.48 < h \leqslant \infty$. Apart from *2.1*, the archipelagos of the three-link trajectory family *3.3* come into being (Fig. 15, $h = 1.5$). For $h > 1.621$, the four-link archipelagos emerge, then the five-link ones and so on. This is already clearly seen in Fig. 16 ($h = 2.0$). Further increase of h leads to more regularity of motions (Fig. 17, $h = 2.5$) and, in the limit $h \to \infty$, the phase maps describe the Birkhoff billiard in the circle (the sets $\dot{\alpha} =$ constant in the plane $(\alpha, \dot{\alpha})$).

We now sum up our investigation of the phase map evolution as h changes, somewhat simplifying matters in order to give an overall description.

1. $-1 < h < 0$. There are oscillatory motions with a high degree of regularity and barely noticeable stochasticity up to $h \approx -0.75$, with developing chaos and number of archipelagos as h further increases. There is a strong stochasticity for $-0.25 \leqslant h \leqslant 0$. One two-link archipelago virtually remains.
2. $0 < h < 1$. There is a very strong global stochasticity of motion with barely noticeable exceptions.
3. $1 < h$. There is a transition to rotatory motions, and the appearance of a large number of regular motion archipelagos in the chaos sea as h increases and there is a high degree of regularity for $h > 2.5$.

Notice that in order to make the presentation more concise, many interesting details are omitted, such as the period-doubling bifurcation as h decreases (for the three-link trajectories for $h = 1.4803$, for the four-link trajectories for $h = 1.621$ and so on) and the analysis of the birth of multi-link trajectories in the vicinity of ones with a small number of links (as in Fig. 15, $h = 1.5$).

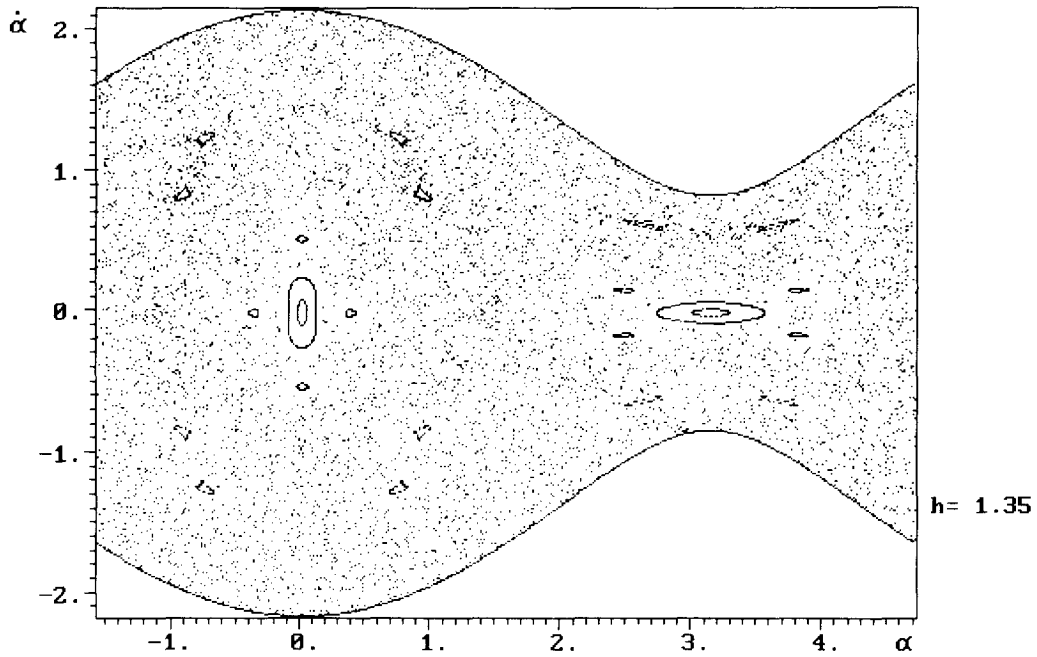

Fig. 14. Surface of section for $h = 1.35$. The family *4.1* transforms into *2.1*.

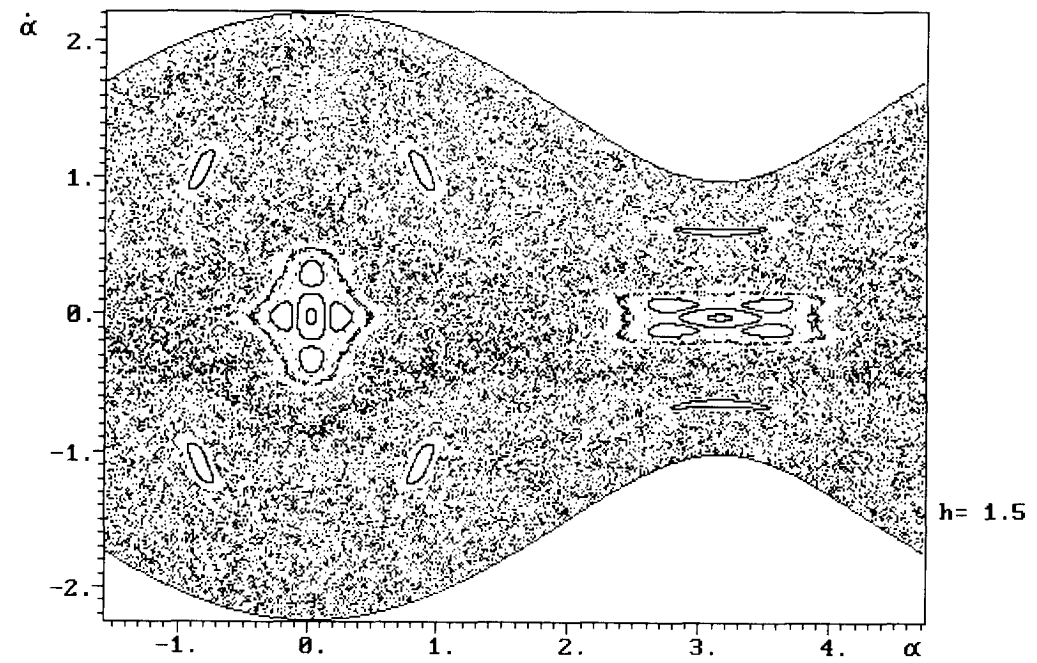

Fig. 15. Surface of section for $h = 1.5$. Chains of the three-link trajectory family *3.3* come into being.

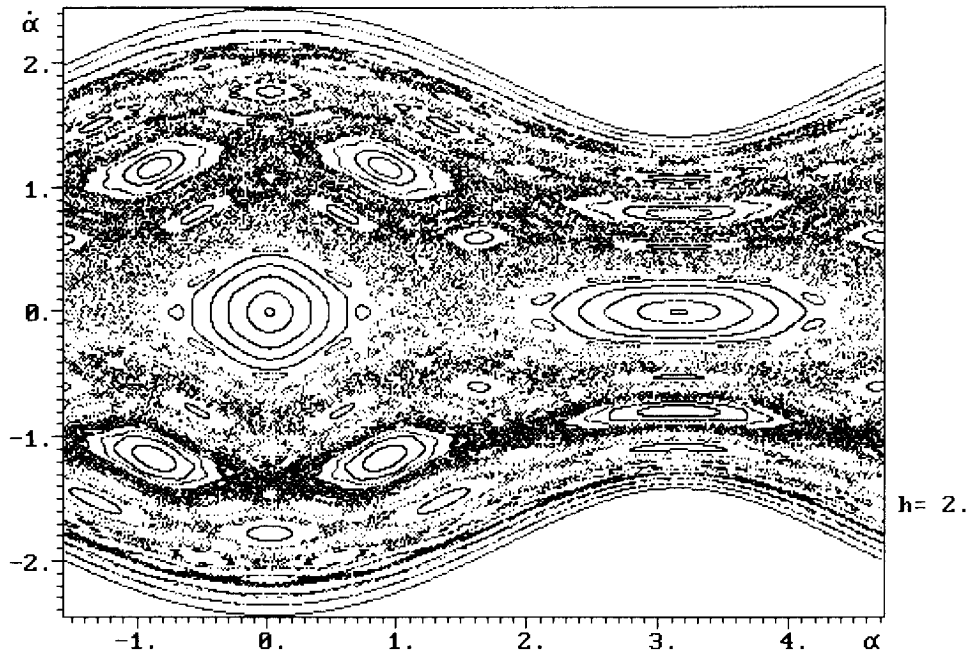

Fig. 16. Surface of section for $h = 2$. The multi-link archipelagos emerge.

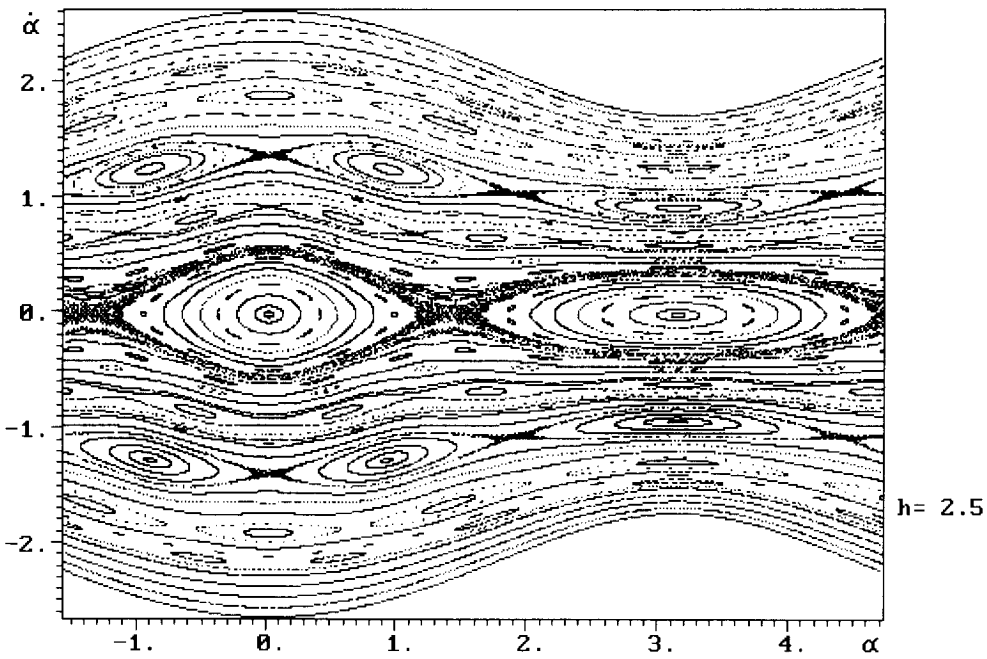

Fig. 17. Surface of section for $h = 2.5$. Further increase in h leads to more regularity of motion.

6. CONSTRAINED MOTIONS AND CONSTRAINT BREAKING

The constrained motion $r = 1$, $\dot{r} = 0$ proceeds in the phase space along the integral curves

$$\tfrac{1}{2}\dot{\alpha}^2 - \cos\alpha = h \tag{29}$$

only if

$$\dot{\alpha}^2 + \cos\alpha > 0. \tag{30}$$

As the inequality (30) is violated, the mass point leaves the constraint and comes off inside the circle. Shown in Fig. 18 are the phase curves (29) and the leaving region, satisfying the opposite sign in the inequality (30), is cross-hatched. It can be seen that the oscillatory motion, for any h in the range $-1 < h < 0$, and the rotatory one, for any $h > 1.5$, proceed without leaving the constraint. For $0 < h < 1.5$, the motion inevitably comes off the constraint and, most likely, to a chaotic trajectory of the gravitating billiard. The stochasticity of the motion after leaving the constraint seems to be probable because (a) there are no billiard trajectories with the initial condition $\dot{r} = 0$ among the periodic ones discussed above, and (b) the range $0 < h < 1.5$ for values of h corresponds to a very strong stochasticity of motion, as is seen from the preceding.

However, there exist periodic trajectories that consist of segments of pendulum-like constrained motion and others consisting of parabolic motion in the interior of the circle. The transition from the constrained motion to the parabolic one occurs on the condition that $r = 1$, $\dot{r} = 0$. One such trajectory is presented in Fig. 19a. The initial conditions at the leaving point are $\alpha_0 = 120°$, $\dot{\alpha}_0 = \sqrt{0.5}$. There also exist periodic trajectories of similar type with larger numbers of links (Fig. 19b). However, they are all likely to be strongly unstable; the slightest change in the initial conditions leads the motion towards chaos.

7. MOTION EVOLUTION ON PERFECTLY INELASTIC CONTACT WITH THE CONSTRAINT

The billiard formulation of the problem made the hypothesis of perfectly elastic contact with the constraint. A partly elastic collision is closer to reality. Of interest is the other

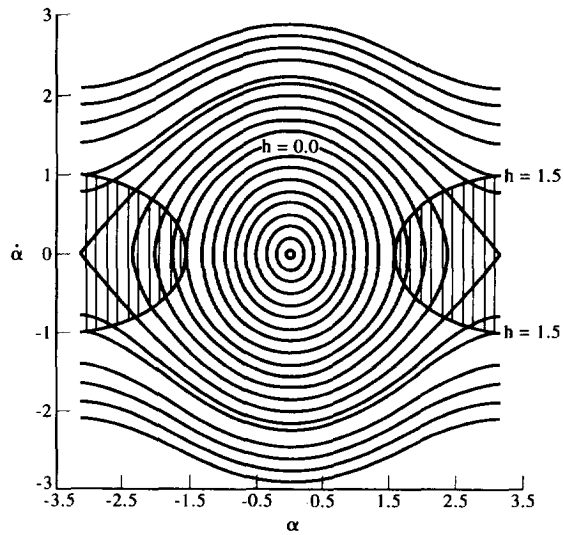

Fig. 18. The phase curves (29) of constrained motion. The leaving region is cross-hatched.

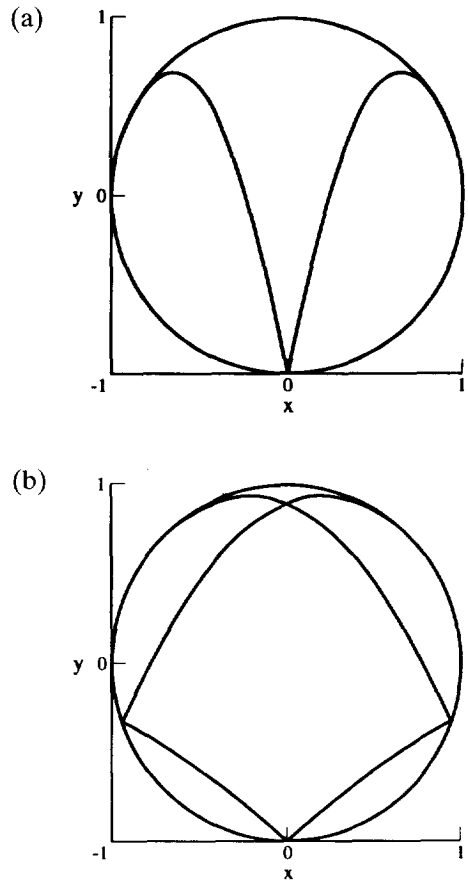

Fig. 19. The periodic trajectories consisting of segments of pendulum-like constrained motion and those consisting of parabolic motion in the interior of the circle. (a) $h = 0.75$. The initial conditions at the leaving point are $\alpha_0 = 120°$, $\dot{\alpha}_0 = \sqrt{(0.5)}$. (b) $h = 1.207$. The trajectory with larger numbers of links.

extreme (limiting) case of perfectly inelastic contact with the constraint. During such a collision, the velocity normal component $\dot{r}$ is cancelled completely, while the tangent component $\dot{\alpha}$ is conserved.

It is clear from the phase map in Fig. 18 that if, after the collision with the constraint, the energy level falls within one of the intervals $-1 < h < 0$ or $h > 1.5$, then the subsequent motion will be of the pendulum-like nature ($\dot{r} \equiv 0$), oscillatory in the first case and rotatory in the second. If, after the perfectly inelastic collision, the motion energy falls within the range $0 < h < 1.5$, then an evolution of motion is possible, of leaving the constraint another time, meeting it again and so on. Let us follow this evolution.† In equation (3), by virtue of the constraint leaving conditions, the constant term and the τ first-order term are equal to zero. Therefore, the instant of subsequent meeting with the constraint is given by $\tau = 4\dot{y}_0$. The phase coordinates at this moment are

$$x = x_0 + 4\dot{x}_0\dot{y}_0, \qquad \dot{x} = \dot{x}_0, \qquad y = y_0 - 4\dot{y}_0^2, \qquad \dot{y} = -3\dot{y}_0.$$

†The results presented below were verified again by students R. Oparina and T. Sitnova from M. V. Lomonosov Moscow State University.

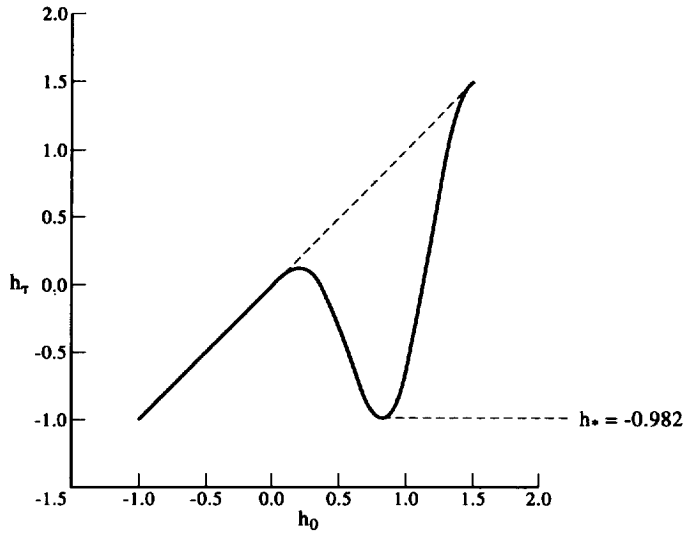

Fig. 20. The energy h_τ after the perfectly inelastic collision vs the energy h_0 before.

The radial (cancelled) velocity v_r and the tangential (conserved) velocity v_τ are evaluated at this moment from the formulas

$$v_r = 8\dot{y}_0^3, \qquad v_\tau^2 = \dot{x}_0^2 + \dot{y}_0^2 + 8\dot{y}_0^2(1 - 8\dot{y}_0^4).$$

The difference of the energies h_τ after the second collision with the circle and h_0 at the instant of the initial escape of the constraint is computed as

$$h_\tau - h_0 = -32\dot{y}_0^6. \tag{31}$$

But $\dot{y}_0$ may be expressed in terms of h_0 as follows:

$$\dot{y}_0^2 = \tfrac{2}{3}h_0(1 - \tfrac{4}{9}h_0^2). \tag{32}$$

By substituting (32) in (31), we finally have

$$h_\tau - h_0 = -\tfrac{256}{27}h_0^3(1 - \tfrac{4}{9}h_0^2)^3. \tag{33}$$

The dependence $h_\tau(h_0)$ given by (33) is presented in Fig. 20. This picture allows us to construct successive maps $h_n \to h_{n+1}$ of the energy from n-th to $(n+1)$-th collision in the energy evolution region. It is obvious that the motion can approach the level $h \equiv 0$ as a limiting cycle, i.e. the pendulum-like motion with an amplitude equal to $\pi/2$. Alternatively, the motion becomes, after one or more collisions, oscillatory with a fixed value of h from the range $h_* \leqslant h < 0$, $h_* \approx -0.982$.

Acknowledgement—The work of two authors (V.B. and E.S.) was partially supported by Russian Foundation of Basic Research grant No. 95–01–00308a.

REFERENCES

1. H. E. Lehtihet and B. N. Miller, Numerical study of a billiard in a gravitational field. *Physica D* **21**, 93–104 (1986).
2. V. I. Arnold, *Méthodes Mathematiques de la Mécanique Classique*. Éditions Mir, Moscow (1976).

3. A. P. Ivanov and A. P. Markeev, On dynamics of systems with unilateral constraints. *Prikladnaya matematika i mekhanika* **48**, 632–636 (1984) (in Russian).
4. V. V. Kozlov and D. V. Treshchyov, *Billiards. A Genetic Introduction into Dynamics of Systems with Collisions*. MGU Publishers, Moscow (1991) (in Russian).
5. A. J. Lichtenberg and M. A. Lieberman, *Regular and Stochastic Motion*. Springer, New York (1983).